

Near-Field Motion Parameter Estimation: A Variational Bayesian Approach

Chunwei Meng, Zhaolin Wang, Zhiqing Wei, Yuanwei Liu, Zhiyong Feng

Abstract—A near-field motion parameter estimation method is proposed. In contrast to far-field sensing systems, the near-field sensing system leverages spherical-wave characteristics to enable full-vector location and velocity estimation. Despite promising advantages, the near-field sensing system faces a significant challenge, where location and velocity parameters are intricately coupled within the signal. To address this challenge, a novel subarray-based variational message passing (VMP) method is proposed for near-field joint location and velocity estimation. First, a factor graph representation is introduced, employing subarray-level directional and Doppler parameters as intermediate variables to decouple the complex location-velocity dependencies. Based on this, the variational Bayesian inference is employed to obtain closed-form posterior distributions of subarray-level parameters. Subsequently, the message passing technique is employed, enabling tractable computation of location and velocity marginal distributions. Two implementation strategies are proposed: 1) System-level fusion that aggregates all subarray posteriors for centralized estimation, or 2) Subarray-level fusion where locally processed estimates from subarrays are fused through Gaussian product rule. Cramér-Rao bounds for location and velocity estimation are derived, providing theoretical performance limits. Numerical results demonstrate that the proposed VMP method outperforms existing approaches while achieving a magnitude lower complexity. Specifically, the proposed VMP method achieves centimeter-level location accuracy and sub-m/s velocity accuracy. It also demonstrates robust performance for high-mobility targets, making the proposed VMP method suitable for real-time near-field sensing and communication applications.

Index Terms—Integrated sensing and communication, joint location and velocity estimation, near-field sensing.

I. INTRODUCTION

The emergence of novel applications in the sixth generation (6G) wireless systems, such as smart manufacturing and intelligent transportation systems, necessitates high-capacity communications and high-precision sensing capabilities [1]–[5]. The demands of these applications make the extremely large-scale multiple-input and multiple-output (XL-MIMO) and millimeter wave (mmWave)/terahertz (THz) technologies key enablers and trends for 6G wireless systems, offering dramatically improved spectral efficiency and spatial resolution. The combination of the two technologies brings paradigm shift in the electromagnetic characteristics of wireless environments [4]. Specifically, the electromagnetic region of the base station

(BS) is divided into near-field and far-field regions by the Rayleigh distance. As the antenna array size increases and the operating frequency increases, the Rayleigh distance extends to hundreds of meters, making it more likely that the BS will carry out communications and sensing in the near-field region [6].

The spherical-wave characteristics of near-field electromagnetic propagation introduce new opportunities for both communication and sensing systems [7]. The potential benefits of near-field communications have been extensively investigated in numerous studies, encompassing spatial multiplexing, inter-user interference management, location division multiple access [6]–[8]. For near-field sensing, the estimation of target parameters, both static and dynamic, is a crucial research problem [9]–[12]. Current research in near-field sensing predominantly focuses on static target localization, leveraging the spatial resolution advantages of spherical wavefronts for enhanced range/angle estimation with reduced time-frequency resources [12]–[15]. However, the paradigm shifts significantly when considering the moving target. Traditional far-field systems using compact arrays can only resolve radial velocity components, while distributed multistatic configurations enable full velocity vector estimation through spatial diversity, albeit at the cost of increased hardware complexity and synchronization requirements [15]–[17]. In [17], the concept of near-field velocity sensing was introduced, enabling a monostatic radar operating in the near-field region to obtain the complete two-dimensional velocity of the target, thus avoiding the requirements for synchronization and the hardware costs associated with multistatic radar systems.

Despite the significant benefits of near-field operations for velocity estimation, research on this topic is still limited. The existing literature can be categorized into two main approaches: filter-based tracking methods and snapshot estimation methods [17]–[19]. In the former category, the authors of [18] proposed a novel near-field sensing enabled predictive beamforming framework that leverages both single-coherent processing interval (CPI) estimation and multi-CPI filtering techniques to estimate the target’s location and velocity. Nevertheless, this approach relies on the availability of continuous CPIs, which may not be feasible for scenarios requiring rapid initial target detection, e.g., the scenario contains newly appearing targets. For the latter category, the authors of [17] investigated the maximum likelihood velocity estimator and its adoption in predictive beamforming applications, assuming known target locations. The reconfigurable intelligent surfaces aided single-snapshot near-field sensing algorithm introduced in [19] decouples the location and velocity estimation utilizing

C. Meng, Z. Wei, and Z. Feng are with the Key Laboratory of Universal Wireless Communications, Ministry of Education, Beijing University of Posts and Telecommunications, Beijing 100876, China (e-mail: {mengchunwei, weizhiqing, fengzy}@bupt.edu.cn). Z. Wang is with the School of Electronic Engineering and Computer Science, Queen Mary University of London, London E1 4NS, U.K. (e-mail: zhaolin.wang@qmul.ac.uk). Y. Liu is with the Department of Electrical and Electronic Engineering, the University of Hong Kong, Hong Kong, China (e-mail: yuanwei@hku.hk).

the static target assumption and linear approximations. However, research on near-field joint location-velocity estimation under unknown initial conditions remains scarce.

The joint estimation of location and velocity for near-field moving targets presents significant challenges when prior information is unavailable, as conventional estimation methods suffer from performance degradation and prohibitive computational complexity when extended to near-field scenarios [17]. This limitation stems from the spherical wavefront effect that creates unique line-of-sight (LoS) direction per antenna-target pair. Consequently, the observed Doppler shifts represent velocity projections along spatially-varying directions, establishing complex nonlinear coupling between target motion parameters and antenna-specific signal characteristics. This inherent coupling necessitates joint parameter estimation, leading to cubic computational complexity scaling with antenna count and snapshots for subspace-based multiple signal classification (MUSIC) algorithms from eigendecomposition, and quartic complexity for compressed sensing methods performing four-dimensional location-velocity parameter space searches. Given that XL-MIMO systems employ hundreds to thousands of antennas, such complexity becomes impractical for real-time moving target estimation.

The transition to near-field sensing in XL-MIMO systems enables reconstructing complete velocity vectors via spherical wavefronts with spatially diverse path projections. However, this advancement faces two critical challenges: 1) The antenna-specific spherical wave curvature induces strong nonlinear coupling between location and velocity parameters, creating complex interdependencies that complicate joint location-velocity estimation; 2) The resulting four-dimensional estimation space imposes prohibitive computational burdens on conventional methods, with complexity scaling combinatorially with array dimensions and observation duration. To overcome these challenges, we develop a novel subarray-based variational message passing (VMP) algorithm for near-field joint location and velocity estimation with computational efficiency. The main contributions of this paper are summarized as follows:

- We propose a novel processing paradigm for near-field joint location and velocity sensing. By partitioning the arrays into subarrays and applying a piecewise-far-field model, each transmit-receive (T-R) subarray pair operates as a bistatic radar. This decouples location and velocity estimation by enabling independent estimation of subarray-level direction parameters and Doppler shifts. Besides, the spherical wavefront propagation across subarrays provides multiperspective spatial diversity, enabling simultaneous 2D location and velocity estimation.
- We introduce direction-of-arrival (DoA), direction of departure (DoD), and bistatic Doppler shift as subarray-level intermediate variables for each T-R subarray pair. Based on this, we establish a probabilistic graphical model that resolves intricate location-velocity dependencies through geometric conditional relationships, enabling efficient separate inference stages. We then develop a variational Bayesian inference (VBI) framework to derive closed-form posterior distributions of subarray-level parameters and estimate crucial hyperparameters, enabling

efficient parallel processing at the subarray level.

- We propose a message passing-based algorithm to achieve efficient joint location-velocity estimation by systematically fusing subarray measurements. The proposed algorithm can operate in two complementary modes: 1) System-level fusion: Performs centralized estimation by integrating all subarray posteriors into a system-level optimization problem solved via gradient descent. 2) Subarray-level fusion: Performs distributed estimation by obtaining subarray-level location and velocity estimates through Laplace approximations, followed by the fusion of Gaussian mixtures to derive the final estimates.
- We evaluate the performance of the proposed method with existing approaches under different scenarios. Numerical results demonstrate that the proposed method achieves centimeter-level localization and sub-m/s velocity accuracy, while achieving an order-of-magnitude reduction in complexity. The proposed system-level fusion achieves higher estimation accuracy, while the subarray-level method offers lower computational complexity through distributed processing. Moreover, the proposed method exhibits robust performance for the high-velocity target, making it suitable for real-time applications.

The rest of this paper is organized as follows. Section II presents the system model, channel model, and problem formulation. Section III establishes the probabilistic model using factor graph representation. Section IV develops the variational inference framework for subarray-level parameter estimation. Section V proposes the variational message passing algorithm for location and velocity estimation. Section VI derives the Cramér-Rao Bound (CRB)s for location and velocity estimation. Section VII presents simulation results and performance evaluation. Finally, Section VIII concludes the paper.

Notation: Vectors and matrices are denoted by boldface lowercase and uppercase letters. $(\cdot)^T$, $(\cdot)^H$, $(\cdot)^{-1}$, and $\|\cdot\|_F$ represent transpose, conjugate transpose, matrix inversion, and Frobenius norm, respectively. $|\cdot|$ and $\|\cdot\|$ denote the absolute value and Euclidean norm, respectively. $\mathcal{CN}(\cdot, \cdot)$, $\mathcal{M}(\cdot, \cdot)$, $\Re\{\cdot\}$, $\Im\{\cdot\}$, $\mathbb{E}\{\cdot\}$, and $\text{tr}\{\cdot\}$ denote complex Gaussian distribution, von Mises distribution, real part operator, imaginary part operator, expectation operator, and trace operator, respectively. \otimes , and \succeq represent Kronecker product and positive semidefinite, respectively. \mathbf{I}_N and $\mathbf{0}$ denote an $N \times N$ identity matrix and a zero matrix. $\delta(\cdot)$ represents the Dirac delta function.

II. SYSTEM MODEL AND PROBLEM FORMULATION

As illustrated in Fig. 1, the BS equipped with transmit and receive XL-uniform linear array (ULA)s actively senses a moving target. The BS's transmit and receive arrays are deployed along the x -axis, symmetrically centered around the origin, and widely separated in space to suppress signal leakage from transmitter. The total number of antenna elements in transmit and receive arrays are N_t and N_r , respectively, with an inter-element spacing of $d = \frac{\lambda}{2}$, where λ denotes the wavelength. Assuming the distance between transmit and receive arrays is D_0 , the location of the i -th transmit antenna is given by $\mathbf{p}_i^t = (\frac{D_0}{2} + (i-1)d, 0)$, and the location of the j -th receive antenna is given by $\mathbf{p}_j^r = (-\frac{D_0}{2} - (j-1)d, 0)$. The

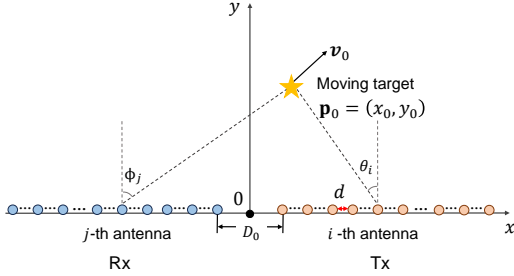


Fig. 1. Illustration of the downlink near-field sensing scenario where the BS equipped with XL-MIMOs senses a moving target in the near-field region.

boundary between the near-field and far-field regions of the BS is determined by the Rayleigh distance, which is given by $R = \min\{\frac{2(N_t-1)^2 d^2}{\lambda}, \frac{2(N_r-1)^2 d^2}{\lambda}\}$. Assume that the moving target is located in the near-field region of both arrays, with its initial location and velocity denoted by $\mathbf{p}_0 = (x_0, y_0)$ and $\mathbf{v}_0 = (v_x, v_y)$, respectively.

Each antenna of the transmitter emits temporally orthogonal signals that impinge on the target, and the reflections are intercepted by the receiver [20]. The signal received at the j -th receive antenna at time t is given by

$$y_j(t) = \sum_{i=1}^{N_t} \beta_{ij} e^{-j \frac{2\pi}{\lambda} [r_{T_i}(t) + r_{R_j}(t)]} s_i(t - \tau_{T_i}(t) - \tau_{R_j}(t)) + n_{ij}(t), \quad (1)$$

where β_{ij} denotes the channel gain, $n_{ij}(t)$ denotes the additive noise which is characterized as i.i.d. complex Gaussian with zero mean and variance σ^2 . The time-variant propagation distances from the i -th transmit antenna to the target and from the j -th receive antenna to the target are represented by $r_{T_i}(t)$ and $r_{R_j}(t)$, respectively. Specifically, we have $r_{T_i}(t) = r_{T_i} + v_i t$ and $r_{R_j}(t) = r_{R_j} + v_j t$, where $r_{T_i} = \|\mathbf{p}_i^t - \mathbf{p}_0\|$ and $r_{R_j} = \|\mathbf{p}_j^r - \mathbf{p}_0\|$ denote initial distances between the target and the i -th transmit antenna and the j -th receive antenna, respectively. The terms v_i and v_j represent the radial velocity components obtained by projecting the target's velocity vector onto the lines connecting the target with the i -th transmit antenna and the j -th receive antenna, respectively. Additionally, $\tau_{T_i}(t) = r_{T_i}(t)/c$ and $\tau_{R_j}(t) = r_{R_j}(t)/c$ are the time delays, where c denotes the speed of light. Following the radar range equation [21], the channel gain β_{ij} can be modeled as $\beta_{ij} = \frac{\sqrt{P_T G_T G_R \alpha_{RCS}}}{r_{T_i} r_{R_j}}$, where P_T is the transmit signal power, G_T represents the antenna gain of the transmit array, G_R represents the antenna gain of the receive array, α_{RCS} is the radar cross section (RCS) of the target, which is modeled as a Swerling I-type fluctuation, remaining constant over the observation interval with $\alpha_{RCS} \sim \mathcal{CN}(0, \sigma_s^2)$ [22].

Considering L pulses within a CPI, the slow-time sampling instants are given by $t_l = lT$ for $l = 0, \dots, L-1$, where T denotes the pulse repetition interval (PRI). Under the common no-range-migration assumption within short CPI [21], the matched filter output at the j -th receive antenna for the i -th transmit antenna and l -th pulse is given by

$$Y_{ij}^{(l)} = \beta_{ij} \exp\left(-j \frac{2\pi}{\lambda} \Phi_{ij}^{(l)}(\mathbf{p}_0, \mathbf{v}_0)\right) + N_{ij}^{(l)}, \quad (2)$$

where the aggregate phase accumulation $\Phi_{ij}^{(l)}(\mathbf{p}_0, \mathbf{v}_0) \in \mathbb{R}$ combines spatial propagation delay and Doppler-induced phase modulation, i.e.,

$$\Phi_{ij}^{(l)}(\mathbf{p}_0, \mathbf{v}_0) \triangleq \underbrace{\|\mathbf{p}_i^t - \mathbf{p}_0\| + \|\mathbf{p}_j^r - \mathbf{p}_0\|}_{\text{Static path delay}} + \underbrace{\lambda t_l f_{ij}(\mathbf{p}_0, \mathbf{v}_0)}_{\text{Dynamic Doppler shift}}. \quad (3)$$

Specifically, the Doppler shift $f_{ij}(\mathbf{p}_0, \mathbf{v}_0)$ for the (i, j) -th T-R antenna pair is given by

$$f_{ij}(\mathbf{p}_0, \mathbf{v}_0) = \frac{1}{\lambda} \left[\frac{[\mathbf{p}_i^t - \mathbf{p}_0]^T \mathbf{v}_0}{\|\mathbf{p}_i^t - \mathbf{p}_0\|} + \frac{[\mathbf{p}_j^r - \mathbf{p}_0]^T \mathbf{v}_0}{\|\mathbf{p}_j^r - \mathbf{p}_0\|} \right]. \quad (4)$$

Therefore, the maximum likelihood estimation requires solving a non-convex optimization, i.e.,

$$\arg \min_{\mathbf{p}_0, \mathbf{v}_0} \sum_{i=1}^{N_t} \sum_{j=1}^{N_r} \sum_{l=1}^L \left| Y_{ij}^{(l)} - \beta_{ij} e^{-j \frac{2\pi}{\lambda} \Phi_{ij}^{(l)}(\mathbf{p}_0, \mathbf{v}_0)} \right|^2. \quad (5)$$

The phase function in (3) induces inseparable nonlinear coupling between \mathbf{p}_0 and \mathbf{v}_0 through each antenna pair, which necessitates 4D joint estimation over (x_0, y_0, v_x, v_y) . This renders the problem (5) computationally intractable due to the exponential complexity scaling with the parameter space dimensionality. To address this limitation, we propose a low-complexity variational Bayesian approach in the following sections, which enables subarray-level distributed processing.

III. PROBABILITY MODEL OF JOINT LOCATION AND VELOCITY ESTIMATION

In this section, we establish the probability model for joint location and velocity estimation problem, leveraging the piecewise-far-field approximation of the near-field channel.

A. Piecewise-Far-Field Channel Model

To decouple the nonlinear interdependency between location and velocity in the phase term (3) while maintaining acceptable accuracy, we employ a piecewise-far-field channel model to approximate the intricate near-field channel [23].

It can be observed that the Rayleigh distance is proportional to the square of the number of antennas, implying that the far-field assumption becomes more accurate for a smaller number of antennas. Consequently, in the piecewise-far-field channel model, we partition the entire transmit and receive arrays into $K_t \triangleq \frac{N_t}{M}$ and $K_r \triangleq \frac{N_r}{N_0}$ non-overlapping subarrays, respectively, where M denotes the number of antennas per subarray. This partitioning creates subarrays with significantly reduced Rayleigh distances (typically meters), enabling far-field planar-wave approximations within individual subarrays while preserving near-field spherical-wave characteristics across subarrays.

Specifically, we select the first antenna of each subarray as the reference antenna to represent the subarray's location. Thus, the position of the m -th transmit subarray is given by $\mathbf{p}_m^t = (x_m^t, y_m^t) = (\frac{D_0}{2} + (m-1)Md, 0)$, and the position of the n -th receive subarray is given by $\mathbf{p}_n^r = (x_n^r, y_n^r) = (-\frac{D_0}{2} - (n-1)Md, 0)$, where $m \in \mathcal{I}_t \triangleq \{1, 2, \dots, K_t\}$ for the transmit array and $n \in \mathcal{I}_r \triangleq \{1, 2, \dots, K_r\}$ for the receive array. Based on the far-field assumption within each

subarray, the DoD $\tilde{\theta}_m$ is defined as the azimuth angle between the target and the m -th transmit subarray's reference antenna, i.e., $\tilde{\theta}_m \triangleq \arctan\left(\frac{x_0 - x_m^t}{y_0 - y_m^t}\right)$, $m \in \mathcal{I}_t$. Similarly, the DoA $\tilde{\phi}_n$ characterizes the arrival angle from the target to the n -th receive subarray at \mathbf{p}_n^r , i.e., $\tilde{\phi}_n \triangleq \arctan\left(\frac{x_0 - x_n^r}{y_0 - y_n^r}\right)$, $n \in \mathcal{I}_r$. Therefore, each T-R subarray pair can be regarded as a traditional bistatic radar. The matched filter output of the received signal for the (m, n) -th T-R subarray pair at the l -th pulse is given by

$$\mathbf{z}_{mn}^{(l)} = \beta_{mn} e^{-j2\pi f_{mn} t_l} \mathbf{a}_r(\phi_n) \otimes \mathbf{a}_t(\theta_m) + \mathbf{n}_{mn}^{(l)}, \quad (6)$$

where $\beta_{mn} \triangleq \frac{\sqrt{P_T G_T G_R \alpha_{RCS}}}{r_{t,m} r_{r,n}}$, with $r_{t,m} \triangleq \|\mathbf{p}_m^t - \mathbf{p}_0\|$ and $r_{r,n} \triangleq \|\mathbf{p}_n^r - \mathbf{p}_0\|$. The bistatic Doppler frequency shift associated with the (m, n) -th T-R subarray pair is represented by f_{mn} , which is given by

$$f_{mn} = -\frac{1}{\lambda} \left[\frac{[\mathbf{p}_m^t - \mathbf{p}_0]^T \mathbf{v}_0}{\|\mathbf{p}_m^t - \mathbf{p}_0\|} + \frac{[\mathbf{p}_n^r - \mathbf{p}_0]^T \mathbf{v}_0}{\|\mathbf{p}_n^r - \mathbf{p}_0\|} \right]. \quad (7)$$

In addition, $\mathbf{a}_t(\theta_m) = [1, e^{j\theta_m}, \dots, e^{j(M-1)\theta_m}]^T$ and $\mathbf{a}_r(\phi_n) = [1, e^{j\phi_n}, \dots, e^{j(M-1)\phi_n}]^T$ denote the m -th transmit and n -th receive subarray steering vectors, respectively, with $\theta_m \triangleq 2\pi d/\lambda \sin \tilde{\theta}_m$ and $\phi_n \triangleq 2\pi d/\lambda \sin \tilde{\phi}_n$. The post-matched-filter noise term $\mathbf{n}_{mn}^{(l)}$ preserves the complex Gaussian distribution [24].

By stacking the slow-time samples $\mathbf{z}_{mn}^{(l)}$ for $t_l = lT$, $l = 0, 1, \dots, L-1$ as columns, we obtain that

$$\mathbf{z}_{mn} = \beta_{mn} \mathbf{a}_r(\phi_n) \otimes \mathbf{a}_t(\theta_m) \otimes \mathbf{d}(f_{mn}) + \mathbf{n}_{mn}, \quad (8)$$

where the complex channel gain β_{mn} follows $\mathcal{CN}(0, \varsigma_{mn})$, and

$$\mathbf{d}(f_{mn}) = [1, e^{-j2\pi f_{mn} T}, \dots, e^{-j2\pi f_{mn} (L-1)T}]^T. \quad (9)$$

B. Probabilistic Model and Factor Graph Representation

Building upon the piecewise-far-field channel model, we now establish the probability model of the joint location and velocity estimation problem. Based on the subarray signal model in (8), the likelihood function of the received signal \mathbf{z}_{mn} given \mathbf{p}_0 , \mathbf{v}_0 and β_{mn} can be expressed as

$$\begin{aligned} p(\mathbf{z}_{mn} | \mathbf{p}_0, \mathbf{v}_0, \beta_{mn}) &= \mathcal{CN}(\mathbf{z}_{mn}; \beta_{mn} \boldsymbol{\mu}_{mn}, \sigma \mathbf{I}_{M^2 L}), \\ &= \frac{1}{(\pi\sigma)^{M^2 L}} \exp\left(-\frac{1}{\sigma} \|\mathbf{z}_{mn} - \beta_{mn} \boldsymbol{\mu}_{mn}\|_2^2\right), \end{aligned} \quad (10)$$

where $\boldsymbol{\mu}_{mn} \triangleq \mathbf{a}_r(\phi_n) \otimes \mathbf{a}_t(\theta_m) \otimes \mathbf{d}(f_{mn})$. By denoting $\boldsymbol{\beta} \triangleq [\beta_{11}, \dots, \beta_{mn}, \dots, \beta_{K_t K_r}]$, the joint probability density function (PDF) is given by

$$\begin{aligned} p(\mathbf{z}, \mathbf{p}_0, \mathbf{v}_0, \boldsymbol{\beta}) &= \prod_{m=1}^{K_t} \prod_{n=1}^{K_r} p(\mathbf{z}_{mn} | \mathbf{p}_0, \mathbf{v}_0, \beta_{mn}) \\ &\quad \times p(\beta_{mn}) p(\mathbf{p}_0) p(\mathbf{v}_0). \end{aligned} \quad (11)$$

Our aim is to find the posteriori distributions $p(\mathbf{p}_0 | \mathbf{z})$ and $p(\mathbf{v}_0 | \mathbf{z})$ and their estimates by using either the minimum mean-square error (MMSE) or maximum a posteriori (MAP) principles. Following the Bayes' theorem, the posterior distri-

butions of \mathbf{p}_0 and \mathbf{v}_0 are given by

$$p(\mathbf{p}_0 | \mathbf{z}) = \int \frac{p(\mathbf{z}, \mathbf{p}_0, \mathbf{v}_0, \boldsymbol{\beta})}{p(\mathbf{z})} d\mathbf{v}_0 d\boldsymbol{\beta}, \quad (12a)$$

$$p(\mathbf{v}_0 | \mathbf{z}) = \int \frac{p(\mathbf{z}, \mathbf{p}_0, \mathbf{v}_0, \boldsymbol{\beta})}{p(\mathbf{z})} d\mathbf{p}_0 d\boldsymbol{\beta}. \quad (12b)$$

However, the coupled nature of \mathbf{p}_0 , \mathbf{v}_0 , and $\boldsymbol{\beta}$ in (11) renders the direct evaluation of the high-dimensional integrals in (12) computationally prohibitive. To resolve the intricate coupling, we introduce intermediate variables ϕ_n (DoA), θ_m (DoD), and f_{mn} (bistatic Doppler frequency) for each T-R subarray pair. By conditioning on these intermediate variables, the likelihood $p(\mathbf{z}_{mn} | \mathbf{p}_0, \mathbf{v}_0, \beta_{mn})$ can be factorized into a cascade of simpler distributions: $p(\mathbf{z}_{mn} | \beta_{mn}, \phi_n, \theta_m, f_{mn})$ and the geometric mappings $p(\phi_n | \mathbf{p}_0)$, $p(\theta_m | \mathbf{p}_0)$, and $p(f_{mn} | \phi_n, \theta_m, \mathbf{v}_0)$, i.e.,

$$\begin{aligned} p(\mathbf{z}, \mathbf{p}_0, \mathbf{v}_0, \boldsymbol{\beta}) &= \prod_{m=1}^{K_t} \prod_{n=1}^{K_r} p(\mathbf{z}_{mn} | \phi_n, \theta_m, f_{mn}, \beta_{mn}) \times \\ &\quad p(f_{mn} | \theta_m, \phi_n, \mathbf{v}_0) p(\mathbf{v}_0) p(\phi_n | \mathbf{p}_0) p(\theta_m | \mathbf{p}_0) p(\mathbf{p}_0) p(\beta_{mn}), \end{aligned} \quad (13)$$

where

$$p(\phi_n | \mathbf{p}_0) = \delta(\phi_n - 2\pi d/\lambda \mathbf{e}(\phi_n)^T \mathbf{e}_x), \quad (14a)$$

$$p(\theta_m | \mathbf{p}_0) = \delta(\theta_m - 2\pi d/\lambda \mathbf{e}(\theta_m)^T \mathbf{e}_x), \quad (14b)$$

$$p(f_{mn} | \phi_n, \theta_m, \mathbf{v}_0) \quad (14c)$$

$$\begin{aligned} &= \delta(f_{mn} - 1/\lambda [\mathbf{v}_0^T \mathbf{e}(\phi_n) + \mathbf{v}_0^T \mathbf{e}(\theta_m)]) \\ &= \delta(f_{mn} - 1/\lambda [v_x \cos \tilde{\theta}_m + v_y \sin \tilde{\theta}_m + v_x \cos \tilde{\phi}_n + v_y \sin \tilde{\phi}_n]), \end{aligned}$$

with

$$\mathbf{e}(\phi_n) \triangleq \frac{(\mathbf{p}_n^r - \mathbf{p}_0)}{\|\mathbf{p}_n^r - \mathbf{p}_0\|}, \quad \mathbf{e}(\theta_m) \triangleq \frac{(\mathbf{p}_m^t - \mathbf{p}_0)}{\|\mathbf{p}_m^t - \mathbf{p}_0\|}. \quad (15)$$

The factorization in (13) can be naturally represented by a factor graph [25], a bipartite graphical model consisting of variable nodes for parameters and factor nodes encoding their probabilistic relationships as detailed in Table I. As shown in Fig. 2, this graphical model explicitly captures the dependencies between motion parameters ($\mathbf{p}_0, \mathbf{v}_0$) and subarray-level variables ($\phi_n, \theta_m, f_{mn}, \beta_{mn}$), enabling the application of VBI (Section IV) and message passing techniques (Section V) for efficient location and velocity estimation.

IV. VARIATIONAL BAYESIAN INFERENCE

In this section, we develop a VBI framework with an alternating optimization algorithm to compute the approximate posterior distributions of subarray-level parameters and estimate the noise variance as well as complex amplitude variance hyperparameters.

Taking the (m, n) -th T-R subarray pair as an example, other subarray pairs can be computed in parallel. Let $\boldsymbol{\Theta} = \{\theta_m, \phi_n, f_{mn}, \beta_{mn}\}$ denote the set of parameters to be estimated in the subarray pair, and $\boldsymbol{\alpha} = \{\varsigma_{mn}, \sigma\}$ represent the hyperparameters. According to Bayesian rule, we have

$$p(\boldsymbol{\Theta} | \mathbf{z}_{mn}; \boldsymbol{\alpha}) \propto \frac{p(\mathbf{z}_{mn}, \boldsymbol{\Theta}; \boldsymbol{\alpha})}{p(\mathbf{z}_{mn}; \boldsymbol{\alpha})}, \quad (16)$$

TABLE I
FACTOR NODES IN FIG. 2

Factor Node	Factor Function
p_{ϕ_n}	$p(\phi_n \mathbf{p}_0) = \delta \left(\phi_n - \frac{(\mathbf{p}_n^t - \mathbf{p}_0)^T \mathbf{e}_y}{\ \mathbf{p}_n^t - \mathbf{p}_0\ } \right)$
p_{θ_m}	$p(\theta_m \mathbf{p}_0) = \delta \left(\theta_m - \frac{(\mathbf{p}_m^t - \mathbf{p}_0)^T \mathbf{e}_y}{\ \mathbf{p}_m^t - \mathbf{p}_0\ } \right)$
$p_{f_{mn}}$	$p(f_{mn} \phi_n, \theta_m, \mathbf{v}_0) = \delta \left(f_{mn} - \frac{1}{\lambda} (\mathbf{v}_0^T \mathbf{e}(\theta_m) + \mathbf{v}_0^T \mathbf{e}(\phi_n)) \right)$
$p_{\beta_{mn}}$	$p(\beta_{mn}) = \mathcal{CN}(\beta_{mn}; 0, \sigma_{mn}^2)$
$p_{z_{mn}}$	$p(\mathbf{z}_{mn} \phi_n, \theta_m, f_{mn}, \beta_{mn}) = \mathcal{CN}(\boldsymbol{\mu}_{mn}, \sigma^2 \mathbf{I}_{M^2L})$

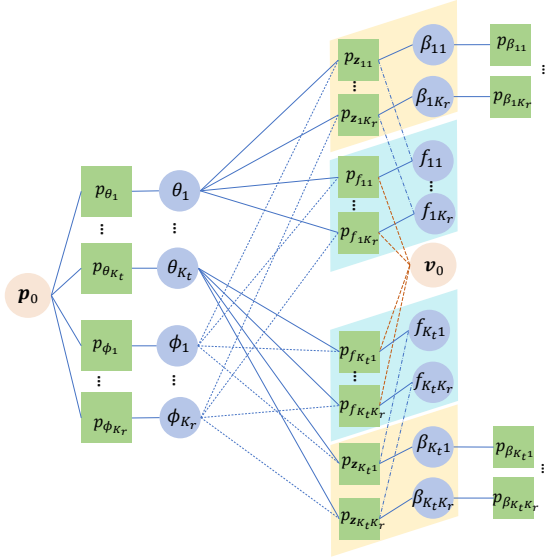


Fig. 2. Factor graph representation of (13), which represents variables as circles and factors as squares, where factors $p(\mathbf{p}_0)$ and $p(\mathbf{v}_0)$ are omitted.

where $p(\mathbf{z}_{mn}; \boldsymbol{\alpha})$ is the model evidence, which acts as a normalizing constant. The numerator $p(\mathbf{z}_{mn}, \boldsymbol{\Theta}; \boldsymbol{\alpha})$ is the joint PDF, which is given by

$$p(\mathbf{z}_{mn}, \boldsymbol{\Theta}; \boldsymbol{\alpha}) = p(\mathbf{z}_{mn} | \boldsymbol{\Theta}; \boldsymbol{\alpha}) p(\theta_m) p(\phi_n) p(f_{mn}) p(\beta_{mn}; \boldsymbol{\alpha}). \quad (17)$$

Calculating the posterior distributions of subarray-level parameters in $\boldsymbol{\Theta}$ is crucial, as they form the basis for the final location and velocity estimates. However, exact Bayesian inference via direct marginalization of the joint posterior in (16) becomes computationally intractable due to the high-dimensional integration and the non-Gaussian nature of angular parameters θ_m , ϕ_n , and Doppler frequency f_{mn} , which precludes closed-form solutions.

Therefore, we resort to the VBI methodology [26], which approximates the true posterior $p(\boldsymbol{\Theta} | \mathbf{z}_{mn}; \boldsymbol{\alpha})$ with a factorized surrogate distribution $q(\boldsymbol{\Theta} | \mathbf{z}_{mn})$ while maintaining computational feasibility. Specifically, we impose a mean-field approximation that factorizes the joint posterior as

$$q(\boldsymbol{\Theta} | \mathbf{z}_{mn}) = q(\theta_m | \mathbf{z}_{mn}) q(\phi_n | \mathbf{z}_{mn}) q(f_{mn} | \mathbf{z}_{mn}) q(\beta_{mn} | \mathbf{z}_{mn}). \quad (18)$$

The optimal surrogate distribution minimizes the Kullback-Leibler divergence (KLD) $D_{KL}(q || p)$, equivalent to maximiz-

ing the evidence lower bound (ELBO):

$$\mathcal{L}(q(\boldsymbol{\Theta} | \mathbf{z}_{mn})) = \mathbb{E}_{q(\boldsymbol{\Theta} | \mathbf{z}_{mn})} \left[\ln \frac{p(\mathbf{z}_{mn}, \boldsymbol{\Theta}; \boldsymbol{\alpha})}{q(\boldsymbol{\Theta} | \mathbf{z}_{mn})} \right]. \quad (19)$$

Then, we solve the optimization of (19) through coordinate ascent variational inference (CAVI) [27], iteratively updating each factor $q(u | \mathbf{z}_{mn})$, $u \in \boldsymbol{\Theta}$ while fixing others. For any parameter $u \in \boldsymbol{\Theta}$, the optimal factor satisfies

$$\ln q(u | \mathbf{z}_{mn}) \propto \mathbb{E}_{\setminus u} [\ln p(\mathbf{z}_{mn}, \boldsymbol{\Theta}; \boldsymbol{\alpha})], \quad (20)$$

where \propto denotes proportionality up to a normalization constant, and $\mathbb{E}_{\setminus u} [\cdot]$ denote the expectation over $\frac{q(\boldsymbol{\Theta} | \mathbf{z}_{mn})}{q(u | \mathbf{z}_{mn})}$.

To enable unified treatment of spatial-temporal parameters, we introduce the normalized Doppler frequency $\tilde{f}_{mn} \triangleq 2\pi T f_{mn}$. This normalized transformation ensures \tilde{f}_{mn} resides on the same $[-\pi, \pi)$ circular domain as ϕ_n and θ_m , permitting unified probabilistic modeling through von Mises (VM) distributions¹. Following variational line spectral estimation principles [28], [29], the VM parameterization enables closed-form variational updates, while inherently circumventing spectral discretization artifacts caused by grid-based compressed sensing approaches. The VM distribution is formally defined as follows.

Definition 1: The VM distribution, denoted as $\mathcal{M}(\theta; \mu, \kappa)$, is a continuous probability distribution defined on the circle, often used to model angular variables [27]. Its probability density function is given by

$$\mathcal{M}(\theta; \mu, \kappa) = \frac{1}{2\pi I_0(\kappa)} \exp(\kappa \cos(\theta - \mu)), \quad (21)$$

where $\theta \in [-\pi, \pi)$ is the angular variable, $\mu \in [-\pi, \pi)$ is the mean direction, $\kappa \geq 0$ is the concentration parameter that controls the concentration of the distribution around the mean, and $I_0(\cdot)$ is the modified Bessel function of the first kind and order zero. Additionally, the VM PDF can also be parameterized in terms of $\eta = \kappa e^{j\mu}$, i.e.,

$$\mathcal{M}(\theta; \eta) = \frac{1}{2\pi I_0(|\eta|)} \exp(\Re\{\eta^* e^{j\theta}\}). \quad (22)$$

A. Inferring the Posterior Probability of $\boldsymbol{\Theta}$

In this subsection, we derive closed-form variational posterior distributions for the parameter set $\boldsymbol{\Theta}$, where parameters $\{\theta_m, \phi_n, \tilde{f}_{mn}\}$ adopt VM distributions while β_{mn} follows

¹The VM distribution is a circular analogue to Gaussian distributions in linear spaces where it serves as the natural exponential family distribution for periodic variables [27].

complex Gaussian distribution, with alternating updates ensuring tractable Bayesian inference.

1) Calculate $q(\phi_n|\mathbf{z}_{mn})$: We maximize \mathcal{L} in (19) w.r.t. $q(\phi_n|\mathbf{z}_{mn})$ when other factors are kept fixed, whose solution follows a VM distribution.

Lemma 1 (Variational VM Posterior for ϕ_n): Under the VM prior $p(\phi_n) = \mathcal{M}(\phi_n; \bar{\eta}_{\phi_n})$, the optimal posterior approximation $q(\phi_n|\mathbf{z}_{mn})$ admits a VM form:

$$q(\phi_n|\mathbf{z}_{mn}) = \mathcal{M}(\phi_n; \hat{\eta}_{\phi_n}), \quad \hat{\eta}_{\phi_n} = \hat{\kappa}_{\phi_n} e^{j\hat{\phi}_n}, \quad (23)$$

where the concentration parameter $\hat{\kappa}_{\phi_n}$ and mean direction $\hat{\phi}_n$ are given by

$$\hat{\phi}_n = \bar{\phi}_n - g'(\bar{\phi}_n)/g''(\bar{\phi}_n) \quad (24a)$$

$$\hat{\kappa}_{\phi_n} = A^{-1}[\exp(1/2g''(\bar{\phi}_n))] \quad (24b)$$

with

$$g(\phi_n) \triangleq \Re(\bar{\eta}_{\phi_n}^* e^{j\phi_n} + \sum_{k=1}^{M-1} \eta_{\phi_n, k}^* e^{jk\phi_n}), \quad (25)$$

where $\tilde{\eta}_{\phi_n, k}^* \triangleq [\boldsymbol{\eta}_{mn}]_{kML:(k+1)ML}^H \hat{\mathbf{c}}_{mn}$, with $\boldsymbol{\eta}_{mn} \triangleq -\frac{2}{\sigma} \mathbf{z}_{mn}$ and $\hat{\mathbf{c}}_{mn} \triangleq \beta_{mn} \mathbf{a}(\hat{\phi}_n) \otimes \mathbf{d}(f_{mn})$. Additionally, $\bar{\phi}_n$ is obtained at the maximum of $g(\phi_n)$, and $A^{-1}(\cdot)$ denoting the inverse of the Bessel ratio function $A(\cdot) = I_1(\cdot)/I_0(\cdot)$ given in [30].

Proof: Please see Appendix A. ■

2) Calculate $q(\theta_m|\mathbf{z}_{mn})$: Following a similar approach, we maximize \mathcal{L} in (19) w.r.t. $q(\theta_m|\mathbf{z}_{mn})$ while fixing other factors.

Lemma 2 (Variational VM Posterior for θ_m): Given the VM prior $p(\theta_m) = \mathcal{M}(\theta_m; \bar{\eta}_{\theta_m})$, the optimal posterior approximation $q(\theta_m|\mathbf{z}_{mn})$ follows a VM distribution, i.e.,

$$q(\theta_m|\mathbf{z}_{mn}) = \mathcal{M}(\theta_m; \hat{\eta}_{\theta_m}), \quad \hat{\eta}_{\theta_m} = \hat{\kappa}_{\theta_m} e^{j\hat{\theta}_m}, \quad (26)$$

where the concentration parameter $\hat{\kappa}_{\theta_m}$ and mean direction $\hat{\theta}_m$ are determined by

$$\hat{\theta}_m = \bar{\theta}_m - g'(\bar{\theta}_m)/g''(\bar{\theta}_m) \quad (27a)$$

$$\hat{\kappa}_{\theta_m} = A^{-1}[\exp(1/2g''(\bar{\theta}_m))] \quad (27b)$$

with

$$g(\theta_m) \triangleq \Re(\bar{\eta}_{\theta_m}^* e^{j\theta_m} + \sum_{k=1}^{M-1} \eta_{\theta_m, k}^* e^{jk\theta_m}), \quad (28)$$

where $\tilde{\eta}_{\theta_m, k}^* \triangleq [\boldsymbol{\eta}_{mn}]_{kML:(k+1)ML}^H \hat{\mathbf{c}}_{mn}^{(1)}$, with $\boldsymbol{\eta}_{mn}^{(1)} \triangleq -\frac{2}{\sigma} \mathbf{z}_{mn}^{(1)}$ and $\hat{\mathbf{c}}_{mn}^{(1)} \triangleq \beta_{mn} \mathbf{a}(\hat{\phi}_n) \otimes \mathbf{d}(\hat{f}_{mn})$. Here, $\mathbf{z}_{mn}^{(1)}$ being a rearrangement of \mathbf{z}_{mn} , and $\bar{\theta}_m$ is obtained at the maximum of $g(\theta_m)$.

Proof: The derivation follows analogous steps to Appendix A by replacing ϕ_n -related variables with θ_m counterparts. ■

3) Calculate $q(\tilde{f}_{mn}|\mathbf{z}_{mn})$: Similar to the derivations for θ_m and ϕ_n , we maximize the ELBO \mathcal{L} w.r.t. $q(\tilde{f}_{mn}|\mathbf{z}_{mn})$ while fixing other factors.

Lemma 3 (Variational VM Posterior for \tilde{f}_{mn}): Under the VM prior $p(\tilde{f}_{mn}) = \mathcal{M}(\tilde{f}_{mn}; \bar{\eta}_{\tilde{f}_{mn}})$, the optimal posterior $q(\tilde{f}_{mn}|\mathbf{z}_{mn})$ follows a VM distribution:

$$q(\tilde{f}_{mn}|\mathbf{z}_{mn}) = \mathcal{M}(\tilde{f}_{mn}; \hat{\eta}_{\tilde{f}_{mn}}), \quad \hat{\eta}_{\tilde{f}_{mn}} = \hat{\kappa}_{\tilde{f}_{mn}} e^{j\hat{f}_{mn}} \quad (29)$$

where the mean direction \hat{f}_{mn} and concentration $\hat{\kappa}_{\tilde{f}_{mn}}$ are:

$$\hat{f}_{mn} = \bar{f}_{mn} - g'(\bar{f}_{mn})/g''(\bar{f}_{mn}) \quad (30a)$$

$$\hat{\kappa}_{\tilde{f}_{mn}} = A^{-1}[\exp(1/2g''(\bar{f}_{mn}))] \quad (30b)$$

with

$$g(\tilde{f}_{mn}) \triangleq \Re(\bar{\eta}_{\tilde{f}_{mn}}^* e^{j\tilde{f}_{mn}} + \sum_{l=1}^{L-1} \eta_{\tilde{f}_{mn}, l}^* e^{jl\tilde{f}_{mn}}), \quad (31)$$

where $\eta_{\tilde{f}_{mn}, l}^* \triangleq (\hat{\mathbf{c}}_{mn}^{(2)})^H [\boldsymbol{\eta}_{mn}^{(2)}]_{lM^2:(l+1)M^2}$, $\boldsymbol{\eta}_{mn}^{(2)} \triangleq -\frac{2}{\sigma} \mathbf{z}_{mn}^{(2)}$, $\mathbf{z}_{mn}^{(2)}$ is a rearrangement of \mathbf{z}_{mn} , and $\hat{\mathbf{c}}_{mn}^{(2)} \triangleq \beta_{mn} \mathbf{a}(\hat{\phi}_n) \otimes \mathbf{a}(\hat{\theta}_m)$. The initial estimate \bar{f}_{mn} corresponds to the maximizer of $g(\tilde{f}_{mn})$.

Proof: Please see Appendix B. ■

4) Calculate $q(\beta_{mn}|\mathbf{z}_{mn})$: We derive the variational posterior for β_{mn} by maximizing the ELBO \mathcal{L} in (19) with respect to $q(\beta_{mn}|\mathbf{z}_{mn})$ while keeping other factors fixed.

Lemma 4 (Variational Gaussian Posterior for β_{mn}): Given the complex Gaussian prior $p(\beta_{mn}) = \mathcal{CN}(0, \varsigma_{mn})$ and likelihood function from (10), the optimal posterior approximation $q(\beta_{mn}|\mathbf{z}_{mn})$ follows a complex Gaussian distribution:

$$q(\beta_{mn}|\mathbf{z}_{mn}) = \mathcal{CN}(\hat{\beta}_{mn}, \tilde{\varsigma}_{mn}) \quad (32)$$

where the posterior mean $\hat{\beta}_{mn}$ and variance $\tilde{\varsigma}_{mn}$ are given by

$$\hat{\beta}_{mn} = \frac{\varsigma_{mn} \boldsymbol{\mu}_{mn}^H \mathbf{z}_{mn}}{\sigma + \varsigma_{mn} \|\boldsymbol{\mu}_{mn}\|_2^2} \quad (33a)$$

$$\tilde{\varsigma}_{mn} = \frac{\varsigma_{mn} \sigma}{2(\sigma + \varsigma_{mn} \|\boldsymbol{\mu}_{mn}\|_2^2)}, \quad (33b)$$

with $\boldsymbol{\mu}_{mn} \triangleq \mathbb{E}_q[\mathbf{a}_r(\phi_n) \otimes \mathbf{a}_t(\theta_m) \otimes \mathbf{d}(f_{mn})]$ denoting the expected steering vector, where the expectation is taken over the variational distributions of ϕ_n , θ_m , and f_{mn} .

Proof: Please see Appendix C. ■

Remark 1: Under non-informative prior conditions, the concentration parameters of the VM priors $p(\phi_n)$, $p(\theta_m)$, and $p(\tilde{f}_{mn})$ can be set close to zero, corresponding to a circular uniform distribution. Similarly, the complex Gaussian prior variance ς_{mn} is set to a large value, approximating an improper uniform prior over the complex plane. This configuration ensures phase wrapping consistency for angular variables and maintains numerical stability during variational updates.

B. Estimating the Hyperparameters α

The noise variance σ and the complex amplitude variance ς_{mn} are typically unknown in practice and must be jointly estimated. Within the variational Bayesian framework, hyperparameter estimation is performed through a coordinate ascent optimization procedure. Specifically, after initializing α , the algorithm iteratively performs variational inference to update $q(\Theta|\mathbf{z}_{mn})$ (Section IV) and computes maximum likelihood estimation (MLE)-type estimates of α by maximizing the ELBO with fixed $q(\Theta|\mathbf{z}_{mn})$.

Lemma 5 (Hyperparameter Estimation via ELBO Maximization): The MLE-type estimates σ and ς_{mn} under the

variational framework yield closed-form solutions, which are given by

$$\hat{\sigma} = \frac{2}{M^2 L} (\|\mathbf{z}_{mn}\|_2^2 + 2\Re(\hat{\beta}_{mn} \mathbf{z}_{mn}^H \boldsymbol{\mu}_{mn}) + \|\boldsymbol{\mu}_{mn}\|_2^2 (\tilde{\zeta}_{mn} + |\hat{\beta}_{mn}|^2)), \quad (34a)$$

$$\hat{\zeta}_{mn} = \tilde{\zeta}_{mn} + |\hat{\beta}_{mn}|^2, \quad (34b)$$

where $\boldsymbol{\mu}_{mn} \triangleq \mathbb{E}_q[\mathbf{a}_r(\phi_n) \otimes \mathbf{a}_t(\theta_m) \otimes \mathbf{d}(f_{mn})]$ represents the expected steering vector, with $\hat{\beta}_{mn}$ and $\tilde{\zeta}_{mn}$ derived from Lemma 4.

Proof: Please see Appendix D. ■

V. PROPOSED MESSAGE PASSING-BASED ESTIMATION ALGORITHM

Building upon the variational posteriors derived in Section IV, we construct a two-tiered message passing architecture that fuses subarray-level parameter estimates into globally consistent motion parameter inference. This framework systematically propagates uncertainty through geometric constraints encoded in the factor graph, where the message operators $\Delta_{a \rightarrow b}(\cdot)$ represent the message from node a to b , while $\Delta_a(\cdot)$ denotes the marginal message at variable node a .

A. Subarray Parameter Estimation Module

We present a unified message passing formulation for joint estimation of direction parameters (DoDs $\{\theta_m\}$, DoAs $\{\phi_n\}$) and bistatic Doppler frequencies $\{f_{mn}\}$ as follows.

Proposition 1 (Unified Message Passing Formulation): For each T-R subarray pair (m, n) , the message from variable node $x \in \{\theta_m, \phi_n, f_{mn}\}$ to its connected factor node p_x admits a closed-form VM distribution:

$$\Delta_{x \rightarrow p_x}(x) \propto \mathcal{M}(x; \mu_{x \rightarrow p_x}, \kappa_{x \rightarrow p_x}), \quad (35)$$

where $\mu_{x \rightarrow p_x}$ and $\kappa_{x \rightarrow p_x}$ represent the mean direction and concentration parameter of the distribution, respectively. The explicit derivations of these parameters are presented in the following.

1) *DoD / DoA Estimation:* According to the sum-product rule [31], the message from variable node θ_m to factor node p_{θ_m} is formulated in (36) at the bottom of this page. Here, $\int_{\setminus \theta_m}$ represents the integration over all variables involved in the message computation, excluding θ_m . Due to the high-dimensional integration, the exact evaluation of $\Delta_{\theta_m \rightarrow p_{\theta_m}}(\theta_m)$ in (36) is computationally intractable.

To alleviate this complexity and enable efficient message passing, we resort to the VM distribution to approximate the messages related to angular variables such as θ_m . By treating the message $\Delta_{p_{\theta_m} \rightarrow \theta_m}(\theta_m)$ as the prior distribution of θ_m , the

expression of (36) can be viewed as an estimate of $p(\mathbf{z}_{mn} | \theta_m)$. Therefore, $\Delta_{\theta_m \rightarrow p_{\theta_m}}(\theta_m)$ can be further expressed as

$$\begin{aligned} \Delta_{\theta_m \rightarrow p_{\theta_m}}(\theta_m) &\propto \frac{\prod_{n=1}^{K_r} p(\mathbf{z}_{mn} | \theta_m) \Delta_{p_{\theta_m} \rightarrow \theta_m}(\theta_m)}{\Delta_{p_{\theta_m} \rightarrow \theta_m}(\theta_m)} \\ &\propto \frac{\prod_{n=1}^{K_r} p(\theta_m | \mathbf{z}_{mn})}{\Delta_{p_{\theta_m} \rightarrow \theta_m}(\theta_m)}, \end{aligned} \quad (37)$$

where the integral is approximated by the posterior distribution $p(\theta_m | \mathbf{z}_{mn})$, which follows a VM distribution, with its explicit form derived in Lemma 2.

The multiplicative closure of VM distributions ensures that the product of $p(\theta_m | \mathbf{z}_{mn})$ also follows a VM distribution, i.e., $\prod_{n=1}^{K_r} p(\theta_m | \mathbf{z}_{mn}) \propto \mathcal{M}(\theta_m; \mu_{\theta_m}, \kappa_{\theta_m})$. Given VM prior with known parameters, the forward message $\Delta_{p_{\theta_m} \rightarrow \theta_m}(\theta_m)$ becomes

$$\Delta_{p_{\theta_m} \rightarrow \theta_m}(\theta_m) \propto \mathcal{M}(\pi \theta_m; \mu_{p_{\theta_m} \rightarrow \theta_m}, \kappa_{p_{\theta_m} \rightarrow \theta_m}), \quad (38)$$

where for unknown priors (non-informative case), we can simply set $\kappa_{p_{\theta_m} \rightarrow \theta_m} \rightarrow 0$.

Then, the message $\Delta_{\theta_m \rightarrow p_{\theta_m}}(\theta_m)$ can be further approximated by

$$\begin{aligned} \Delta_{\theta_m \rightarrow p_{\theta_m}}(\theta_m) &\propto \frac{\mathcal{M}(\theta_m; \mu_{\theta_m}, \kappa_{\theta_m})}{\mathcal{M}(\theta_m; \mu_{p_{\theta_m} \rightarrow \theta_m}, \kappa_{p_{\theta_m} \rightarrow \theta_m})} \\ &\propto \mathcal{M}(\theta_m; \mu_{\theta_m \rightarrow p_{\theta_m}}, \kappa_{\theta_m \rightarrow p_{\theta_m}}), \end{aligned} \quad (39)$$

where the parameters $\mu_{\theta_m \rightarrow p_{\theta_m}}$ and $\kappa_{\theta_m \rightarrow p_{\theta_m}}$ are obtained by

$$\begin{aligned} \kappa_{\theta_m \rightarrow p_{\theta_m}} \exp(j\mu_{\theta_m \rightarrow p_{\theta_m}}) &= \kappa_{\theta_m} \exp(j\mu_{\theta_m}) - \\ &\quad \kappa_{p_{\theta_m} \rightarrow \theta_m} \exp(j\mu_{p_{\theta_m} \rightarrow \theta_m}). \end{aligned} \quad (40)$$

Similarly, the message $\Delta_{\phi_n \rightarrow p_{\phi_n}}(\phi_n)$ can also be approximated by a VM distribution, which is given by

$$\Delta_{\phi_n \rightarrow p_{\phi_n}}(\phi_n) \propto \mathcal{M}(\phi_n; \mu_{\phi_n \rightarrow p_{\phi_n}}, \kappa_{\phi_n \rightarrow p_{\phi_n}}). \quad (41)$$

2) *Bistatic Doppler Estimation:* The bistatic Doppler frequency estimation follows analogous message passing with angular parameters. The message propagating from variable node f_{mn} to factor node $p_{f_{mn}}$ is formulated by

$$\begin{aligned} \Delta_{f_{mn} \rightarrow p_{f_{mn}}}(f_{mn}) &\propto \frac{p(\mathbf{z}_{mn} | f_{mn}) \Delta_{p_{f_{mn}} \rightarrow f_{mn}}(f_{mn})}{\Delta_{p_{f_{mn}} \rightarrow f_{mn}}(f_{mn})} \\ &\propto \frac{p(f_{mn} | \mathbf{z}_{mn})}{\Delta_{p_{f_{mn}} \rightarrow f_{mn}}(f_{mn})}, \end{aligned} \quad (42)$$

where $\Delta_{p_{f_{mn}} \rightarrow f_{mn}}$ is treated as an approximation of the prior distribution of f_{mn} , which can also be modeled by a VM distribution, i.e., $\Delta_{p_{f_{mn}} \rightarrow f_{mn}}(f_{mn}) \propto \mathcal{M}(2\pi T f_{mn}; \mu_{p_{f_{mn}} \rightarrow f_{mn}}, \kappa_{p_{f_{mn}} \rightarrow f_{mn}})$.

Therefore, the message $\Delta_{f_{mn} \rightarrow p_{f_{mn}}}(f_{mn})$ can be further

$$\begin{aligned} \Delta_{\theta_m \rightarrow p_{\theta_m}}(\theta_m) &\propto \prod_{n=1}^{K_r} \int_{\setminus \theta_m} p(\mathbf{z}_{mn} | \phi_n, \theta_m, f_{mn}, \beta_{mn}) \Delta_{\beta_{mn} \rightarrow p_{z_{mn}}}(\beta_{mn}) \Delta_{f_{mn} \rightarrow p_{z_{mn}}}(f_{mn}) \Delta_{\phi_n \rightarrow p_{z_{mn}}}(\phi_n) \\ &\quad \times \prod_{n=1}^{K_r} \int_{\setminus \theta_m} p(f_{mn} | \phi_n, \theta_m, \mathbf{v}_0) \Delta_{f_{mn} \rightarrow p_{f_{mn}}}(f_{mn}) \Delta_{\mathbf{v}_0 \rightarrow p_{f_{mn}}}(\mathbf{v}_0) \Delta_{\phi_n \rightarrow p_{f_{mn}}}(\phi_n). \end{aligned} \quad (36)$$

approximated by VM distribution, which is given by

$$\begin{aligned} \Delta_{f_{mn} \rightarrow p_{f_{mn}}}(f_{mn}) &\propto \frac{\mathcal{M}(2\pi T f_{mn}; \mu_{f_{mn}}, \kappa_{f_{mn}})}{\mathcal{M}(2\pi T f_{mn}; \mu_{p_{f_{mn}} \rightarrow f_{mn}}, \kappa_{p_{f_{mn}} \rightarrow f_{mn}})}, \\ &\propto \mathcal{M}(2\pi T f_{mn}; \mu_{f_{mn} \rightarrow p_{f_{mn}}}, \kappa_{f_{mn} \rightarrow p_{f_{mn}}}), \end{aligned} \quad (43)$$

where $\mu_{f_{mn}}$ and $\kappa_{f_{mn}}$ can be calculated by Lemma 3. Then, the final parameters $\mu_{\theta_m \rightarrow p_{\theta_m}}$ and $\kappa_{\theta_m \rightarrow p_{\theta_m}}$ are obtained by

$$\begin{aligned} &\kappa_{f_{mn} \rightarrow p_{f_{mn}}} \exp(j\mu_{f_{mn} \rightarrow p_{f_{mn}}}) \\ &= \kappa_{f_{mn}} \exp(j\mu_{f_{mn}}) - \kappa_{p_{f_{mn}} \rightarrow f_{mn}} \exp(j\mu_{p_{f_{mn}} \rightarrow f_{mn}}). \end{aligned} \quad (44)$$

B. Location Estimation Module

The spherical wavefront diversity across subarrays creates geometrically distinct observation perspectives, enabling two complementary localization strategies. The first strategy employs a centralized framework that aggregates all posterior distributions for DoAs and DoDs in a central processor for final location estimation. The second strategy adopts a distributed framework where each T-R subarray pair independently resolves local position estimates, which are then fused to obtain the final estimate.

1) *Centralized Location Estimation:* The centralized fusion framework propagates directional evidence from all T-R subarray pairs through geometric constraints in the factor graph. Based on VM-form messages $\Delta_{\theta_m \rightarrow p_{\theta_m}}$ and $\Delta_{\phi_n \rightarrow p_{\phi_n}}$ obtained in (39) and (41), the messages from p_{θ_m} to \mathbf{p}_0 can be given by

$$\begin{aligned} \Delta_{p_{\theta_m} \rightarrow \mathbf{p}_0}(\mathbf{p}_0) &\propto \int_{\theta_m} p(\theta_m | \mathbf{p}_0) \Delta_{\theta_m \rightarrow p_{\theta_m}}(\theta_m), \\ &\propto \mathcal{M}\left(\frac{(\mathbf{p}_m^t - \mathbf{p}_0)^T \mathbf{e}_y}{\|\mathbf{p}_m^t - \mathbf{p}_0\|}; \mu_{\theta_m \rightarrow p_{\theta_m}}, \kappa_{\theta_m \rightarrow p_{\theta_m}}\right). \end{aligned} \quad (45)$$

Similarly, the messages from p_{ϕ_n} to \mathbf{p}_0 can be given by

$$\begin{aligned} \Delta_{p_{\phi_n} \rightarrow \mathbf{p}_0}(\mathbf{p}_0) &\propto \int_{\phi_n} p(\phi_n | \mathbf{p}_0) \Delta_{\phi_n \rightarrow p_{\phi_n}}(\phi_n), \\ &\propto \mathcal{M}\left(\frac{(\mathbf{p}_n^r - \mathbf{p}_0)^T \mathbf{e}_y}{\|\mathbf{p}_n^r - \mathbf{p}_0\|}; \mu_{\phi_n \rightarrow p_{\phi_n}}, \kappa_{\phi_n \rightarrow p_{\phi_n}}\right). \end{aligned} \quad (46)$$

Therefore, the marginal probability distribution of \mathbf{p}_0 can be computed by the product of all the factor node messages connected to \mathbf{p}_0 , i.e.,

$$\Delta_{\mathbf{p}_0}(\mathbf{p}_0) \propto \prod_{m=1}^{K_t} \prod_{n=1}^{K_r} \Delta_{p_{\theta_m} \rightarrow \mathbf{p}_0}(\mathbf{p}_0) \Delta_{p_{\phi_n} \rightarrow \mathbf{p}_0}(\mathbf{p}_0). \quad (47)$$

Based on the central limit theorem, the message $\mathcal{G}(\mathbf{p}_0)$ can be approximated as a Gaussian distribution as

$$\Delta_{\mathbf{p}_0}(\mathbf{p}_0) \propto \mathcal{N}(\mathbf{p}_0; \mathbf{m}_G, \mathbf{C}_G), \quad (48)$$

where \mathbf{m}_G is the mean vector, and \mathbf{C}_G is the covariance matrix, which are obtained in Appendix E.

2) *Distributed Location Estimation:* For each subarray pair (m, n) , the local marginal distribution of \mathbf{p}_0 is given by

$$\Delta_{\mathbf{p}_0}^{(mn)}(\mathbf{p}_0) \propto \Delta_{p_{\theta_m} \rightarrow \mathbf{p}_0}(\mathbf{p}_0) \Delta_{p_{\phi_n} \rightarrow \mathbf{p}_0}(\mathbf{p}_0). \quad (49)$$

By applying the Laplace approximation for the product of $\Delta_{p_{\theta_m} \rightarrow \mathbf{p}_0}(\mathbf{p}_0)$ and $\Delta_{p_{\phi_n} \rightarrow \mathbf{p}_0}(\mathbf{p}_0)$, we can obtain the Gaussian

approximation of (49), i.e.,

$$\Delta_{\mathbf{p}_0}^{(mn)}(\mathbf{p}_0) \propto \mathcal{N}(\mathbf{p}_0; \mathbf{m}_p^{(mn)}, \mathbf{C}_p^{(mn)}), \quad (50)$$

where $\mathbf{m}_p^{(mn)}$ and $\mathbf{C}_p^{(mn)}$ are provided in Appendix F.

The final posterior distribution of the target location \mathbf{p}_0 is obtained by fusing the marginal distributions (50) from all T-R subarray pairs through a product of Gaussians, i.e., $\prod_{m=1}^{K_t} \prod_{n=1}^{K_r} \Delta_{\mathbf{p}_0}^{(mn)}(\mathbf{p}_0)$. The resulting distribution is a Gaussian with mean vector and covariance matrix given by

$$\tilde{\mathbf{m}}_G = \tilde{\mathbf{C}}_G \sum_{m,n} (\mathbf{C}_p^{(mn)})^{-1} \mathbf{m}_p^{(mn)}, \quad (51a)$$

$$\tilde{\mathbf{C}}_G^{-1} = \sum_{m,n} (\mathbf{C}_p^{(mn)})^{-1}. \quad (51b)$$

C. Velocity Estimation Module

The velocity estimation process exploits diverse Doppler frequencies across T-R subarray pairs, employing centralized and distributed strategies.

1) *Centralized Velocity Estimation:* For each subarray pair (m, n) , the message from the factor node $p_{f_{mn}}$ to the variable node \mathbf{v}_0 is given by

$$\Delta_{p_{f_{mn}} \rightarrow \mathbf{v}_0}(\mathbf{v}_0) \propto \int_{\setminus \mathbf{v}_0} p(f_{mn} | \phi_n, \theta_m, \mathbf{v}_0) \times \quad (52)$$

$$\Delta_{\theta_m \rightarrow p_{f_{mn}}}(\theta_m) \Delta_{\phi_n \rightarrow p_{f_{mn}}}(\phi_n) \Delta_{f_{mn} \rightarrow p_{f_{mn}}}(f_{mn}),$$

where ϕ_n and θ_m are treated as known parameters and set to their most probable values when estimating the velocity \mathbf{v}_0 . Then, the messages $\Delta_{\theta_m \rightarrow p_{f_{mn}}}(\theta_m)$ and $\Delta_{\phi_n \rightarrow p_{f_{mn}}}(\phi_n)$ can be ignored as constants when evaluated at their maximum probability values $\hat{\theta}_m = \mu_{\theta_m \rightarrow p_{f_{mn}}}$ and $\hat{\phi}_n = \mu_{\phi_n \rightarrow p_{f_{mn}}}$. Therefore, the message in (52) can be simplified by

$$\Delta_{p_{f_{mn}} \rightarrow \mathbf{v}_0}(\mathbf{v}_0) \propto \Delta_{f_{mn} \rightarrow p_{f_{mn}}}(\zeta \mathbf{v}_0^T \mathbf{u}_{mn}), \quad (53)$$

where $\zeta \triangleq 2\pi T/\lambda$, and $\mathbf{u}_{mn} \triangleq \mathbf{e}(\phi_n) + \mathbf{e}(\theta_m)$ represents the sum of the unit direction vectors corresponding to the estimated DoD $\hat{\theta}_m$ and DoA $\hat{\phi}_n$.

Based on (53), the marginal probability distribution of \mathbf{v}_0 can be obtained by

$$\Delta_{\mathbf{v}_0}(\mathbf{v}_0) \propto \prod_{m=1}^{K_t} \prod_{n=1}^{K_r} \Delta_{f_{mn} \rightarrow p_{f_{mn}}}(\zeta \mathbf{v}_0^T \mathbf{u}_{mn}). \quad (54)$$

By applying the Laplace approximation, we can obtain a Gaussian approximation of $\Delta_{\mathbf{v}_0}(\mathbf{v}_0)$, which is given by

$$\Delta_{\mathbf{v}_0}(\mathbf{v}_0) \propto \mathcal{CN}(\mathbf{v}_0; \mathbf{m}_H, \mathbf{C}_H), \quad (55)$$

where the mean vector \mathbf{m}_H and the covariance matrix \mathbf{C}_H are given in Appendix G.

2) *Distributed Velocity Estimation:* In contrast to location estimation, the ambiguity in the velocity vector direction arises when using a single subarray pair. To resolve this problem, we employ geometric diversity through distinct T-R subarray configurations. Let Ω denote the set of all possible configurations of two distinct T-R subarray pairs, with each configuration represented by $\omega_i = \{(m, n), (p, q)\}$, where $i = 1, 2, \dots, |\Omega|$, and $|\Omega|$ represents the total number of configurations. To address the velocity estimation issue, we select a subset of configurations $\omega_i \in \Omega$, such that $m \neq p$ or

$n \neq q$, to obtain the marginal distributions of \mathbf{v}_0 . The marginal distribution of \mathbf{v}_0 determined by the configuration ω_i is given by

$$\Delta_{\mathbf{v}_0}^{(\omega_i)}(\mathbf{v}_0) \propto \Delta_{f_{mn} \rightarrow p_{f_{mn}}}(\zeta \mathbf{v}_0^T \mathbf{u}_{mn}) \Delta_{f_{pq} \rightarrow p_{f_{pq}}}(\zeta \mathbf{v}_0^T \mathbf{u}_{pq}). \quad (56)$$

By applying the Laplace approximation for the product of $\Delta_{f_{mn} \rightarrow p_{f_{mn}}}(\zeta \mathbf{v}_0^T \mathbf{u}_{mn})$ and $\Delta_{f_{pq} \rightarrow p_{f_{pq}}}(\zeta \mathbf{v}_0^T \mathbf{u}_{pq})$, we can obtain the Gaussian approximation of $\Delta_{\mathbf{v}_0}^{(\omega_i)}(\mathbf{v}_0)$, i.e.,

$$\Delta_{\mathbf{v}_0}^{(\omega_i)}(\mathbf{p}_0) \propto \mathcal{N}(\mathbf{p}_0; \mathbf{m}_v^{(\omega_i)}, \mathbf{C}_v^{(\omega_i)}), \quad (57)$$

where $\mathbf{m}_v^{(\omega_i)}$ and $\mathbf{C}_v^{(\omega_i)}$ are given in Appendix H.

Subsequently, distributions in (57) are fused by a product of Gaussians to acquire the final velocity estimate, where the mean vector and covariance matrix given by:

$$\tilde{\mathbf{m}}_{\mathcal{H}} = \tilde{\mathbf{C}}_{\mathcal{H}} \left(\sum_{i=1}^{|\Omega|} (\mathbf{C}_v^{(\omega_i)})^{-1} \mathbf{m}_v^{(\omega_i)} \right), \quad (58a)$$

$$\tilde{\mathbf{C}}_{\mathcal{H}}^{-1} = \sum_{i=1}^{|\Omega|} (\mathbf{C}_v^{(\omega_i)})^{-1}. \quad (58b)$$

D. Overall Algorithm

Based on previous sections, we propose the Variational Inference and Message Passing-based Near-Field Motion Parameter Estimation (VMP-NMPE) algorithm, as summarized in Algorithm 2 and illustrated in Fig. 3. The proposed framework operates through two cascaded stages:

Stage 1 - Variational Bayesian Inference: Each T-R subarray pair executes parallel computation of closed-form posterior distributions for intermediate parameters (DoA ϕ_n , DoD θ_m , bistatic Doppler f_{mn} , reflection coefficient β_{mn}) and hyperparameters (σ , ζ_{mn}) through CAVI, as summarized in Algorithm 1.

Stage 2 - Hierarchical Message Passing: A two-tiered message passing architecture, which contains two modes:

- *System-level fusion:* Aggregates all subarray messages through gradient-based optimization for centralized location and velocity estimation.
- *Subarray-level fusion:* Performs distributed estimation, fusing results via Gaussian mixture product rules to obtain final location and velocity estimates.

The computational complexity of the VMP-NMPE algorithm is as follows: The variational inference stage requires $O(K_t K_r N_{vi} (M^2 + ML))$ operations for N_{vi} iterations across $K_t K_r$ subarrays. The location estimation via system-level fusion involves $O(N_{gd} K_t K_r)$ operations for gradient descent with N_{gd} steps, while the velocity estimation entails $O(N_{ga} K_t K_r)$ operations for Gauss-Newton iterations with N_{ga} steps. The subarray-level distributed fusion incurs $O(|\Omega|)$ operations for $|\Omega|$ subarray pair configurations.

VI. CRAMER-RAO BOUND

To evaluate the near-field motion parameter estimation, we derive the CRBs for estimating $\boldsymbol{\eta} = [\mathbf{p}_0^T, \mathbf{v}_0^T, \tilde{\boldsymbol{\beta}}^T]^T$. We first define an intermediate parameter set $\boldsymbol{\rho} = [\boldsymbol{\theta}^T, \boldsymbol{\phi}^T, \mathbf{f}^T, \tilde{\boldsymbol{\beta}}^T]^T$, where $\boldsymbol{\theta} \triangleq [\theta_1, \dots, \theta_{K_t}]$, $\boldsymbol{\phi} \triangleq [\phi_1, \dots, \phi_{K_r}]$, $\mathbf{f} \triangleq [f_{11}, f_{12}, \dots, f_{K_t K_r}]$, and $\tilde{\boldsymbol{\beta}} \triangleq [\Re\{\beta_{11}\}, \dots, \Re\{\beta_{K_t K_r}\}, \Im\{\beta_{11}\}, \dots, \Im\{\beta_{K_t K_r}\}]$.

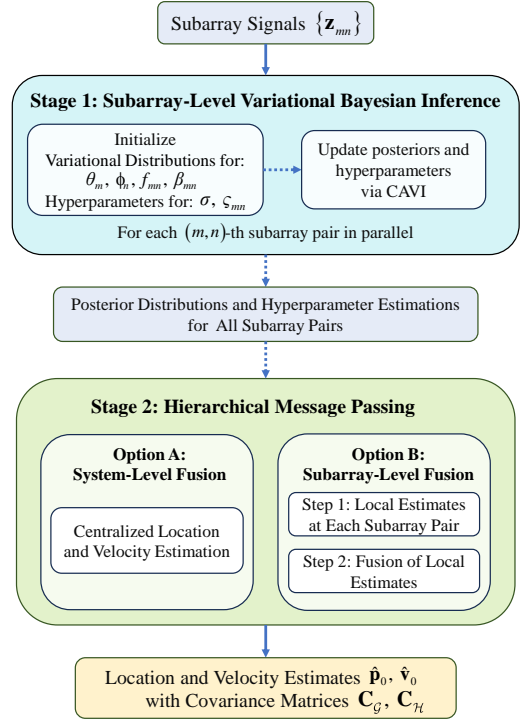


Fig. 3. Flow diagram of the proposed VMP-NMPE Algorithm.

Algorithm 1 Variational Bayesian Inference for Subarray Pair

Require: \mathbf{z}_{mn} , $\bar{\eta}_{\theta_m}$, $\bar{\eta}_{\phi_n}$, $\bar{\eta}_{f_{mn}}$, $\zeta_{mn}^{(0)}$, $\hat{\beta}_{mn}^{(0)}$, $\sigma^{(0)}$, ϵ

Ensure: Posterior parameters $\hat{\eta}_{\theta_m}$, $\hat{\eta}_{\phi_n}$, $\hat{\eta}_{f_{mn}}$, $\hat{\beta}_{mn}$, and hyperparameters ζ_{mn} , $\hat{\sigma}$

- 1: Initialize $q^{(0)}(\theta_m) \leftarrow \mathcal{M}(\theta_m; \bar{\eta}_{\theta_m})$
- 2: Initialize $q^{(0)}(\phi_n) \leftarrow \mathcal{M}(\phi_n; \bar{\eta}_{\phi_n})$
- 3: Initialize $q^{(0)}(f_{mn}) \leftarrow \mathcal{M}(f_{mn}; \bar{\eta}_{f_{mn}})$
- 4: Initialize $q^{(0)}(\beta_{mn}) \leftarrow \mathcal{CN}(0, \zeta_{mn}^{(0)})$
- 5: Initialize $\boldsymbol{\xi}^{(0)} \leftarrow [\bar{\eta}_{\theta_m}, \bar{\eta}_{\phi_n}, \bar{\eta}_{f_{mn}}, \hat{\beta}_{mn}^{(0)}, \zeta_{mn}^{(0)}, \hat{\sigma}^{(0)}]$
- 6: **for** $i = 1$ to N_{\max} **do**
- 7: Update angular posteriors: $\hat{\eta}_{\phi_n}^{(i)} \leftarrow \text{Solve (23)}$, $\hat{\eta}_{\theta_m}^{(i)} \leftarrow \text{Solve (26)}$,
- 8: Update Doppler posterior: $\hat{\eta}_{f_{mn}}^{(i)} \leftarrow \text{Solve (29)}$
- 9: Update reflection coefficient: $\hat{\beta}_{mn}^{(i)}, \zeta_{mn}^{(i)} \leftarrow \text{(33a)-(33b)}$
- 10: Estimate hyperparameters: $\hat{\sigma}^{(i)} \leftarrow \text{(34a)}$, $\zeta_{mn}^{(i)} \leftarrow \text{(34b)}$
- 11: Update $\boldsymbol{\xi}^{(i)} \leftarrow [\hat{\eta}_{\theta_m}^{(i)}, \hat{\eta}_{\phi_n}^{(i)}, \hat{\eta}_{f_{mn}}^{(i)}, \hat{\beta}_{mn}^{(i)}, \zeta_{mn}^{(i)}, \hat{\sigma}^{(i)}]$
- 12: **if** $\|\boldsymbol{\xi}^{(i)} - \boldsymbol{\xi}^{(i-1)}\| < \epsilon$ **then**
- 13: **break**
- 14: **end if**
- 15: **end for**

The CRB for $\boldsymbol{\eta}$ satisfies

$$\mathbb{E}\{(\hat{\boldsymbol{\eta}} - \boldsymbol{\eta})(\hat{\boldsymbol{\eta}} - \boldsymbol{\eta})^T\} \succeq \mathbf{F}_{\boldsymbol{\eta}}^{-1}, \quad (59)$$

where $\mathbf{F}_{\boldsymbol{\eta}}$ denotes the Fisher information matrix (FIM) for $\boldsymbol{\eta}$, which is given by

$$\mathbf{F}_{\boldsymbol{\eta}} = \frac{2}{\sigma} \sum_{m=1}^{K_t} \sum_{n=1}^{K_r} \sum_{l=0}^{L-1} \Re \left\{ \left(\frac{\partial(\beta_{mn} \boldsymbol{\mu}_{mn}^{(l)})}{\partial \boldsymbol{\eta}} \right)^H \left(\frac{\partial(\beta_{mn} \boldsymbol{\mu}_{mn}^{(l)})}{\partial \boldsymbol{\eta}} \right) \right\}. \quad (60)$$

Algorithm 2 VMP-NMPE: Variational Message Passing for Near-Field Motion Parameter Estimation

Require: $\{\mathbf{z}_{mn}\}$, system parameters T, λ , convergence thresholds $\epsilon, \epsilon_1, \epsilon_2$

Ensure: Target location $\hat{\mathbf{p}}_0$, velocity $\hat{\mathbf{v}}_0$, covariance matrices $\mathbf{C}_G, \mathbf{C}_H$

- 1: **Stage 1: Distributed Variational Inference**
 - 2: **for** each transmit subarray $m \in [1, K_t]$ **do**
 - 3: **for** each receive subarray $n \in [1, K_r]$ **do**
 - 4: Run Algorithm 1 for subarray pair (m, n)
 - 5: Store posterior parameters $\hat{\eta}_{\theta_m}, \hat{\eta}_{\phi_n}, \hat{\eta}_{f_{mn}}, \hat{\beta}_{mn}$
 - 6: Compute local messages $\Delta_{p_{\theta_m} \rightarrow \theta_m}, \Delta_{p_{\phi_n} \rightarrow \phi_n}, \Delta_{p_{f_{mn}} \rightarrow f_{mn}}$ using (35)
 - 7: **end for**
 - 8: **end for**
 - 9: **Stage 2: Hierarchical Message Passing**
 - 10: **Option A: System-level Fusion**
 - 11: Initialize $\mathbf{p}_0^{(0)}$, set iteration $i = 0$
 - 12: **while** $\|\mathbf{p}_0^{(i+1)} - \mathbf{p}_0^{(i)}\| > \epsilon_1$ **do**
 - 13: Update $\mathbf{p}_0^{(i+1)}$ using (E.5)
 - 14: $i \leftarrow i + 1$
 - 15: **end while**
 - 16: Set $\hat{\mathbf{p}}_0 = \mathbf{p}_0^{(i)}$, compute \mathbf{C}_G using (E.9)
 - 17: Initialize $\mathbf{v}_0^{(0)}$, set iteration $j = 0$
 - 18: **while** $\|\mathbf{v}_0^{(j+1)} - \mathbf{v}_0^{(j)}\| > \epsilon_2$ **do**
 - 19: Update $\mathbf{v}_0^{(j+1)}$ using (G.3)
 - 20: $j \leftarrow j + 1$
 - 21: **end while**
 - 22: Set $\hat{\mathbf{v}}_0 = \mathbf{v}_0^{(j)}$, compute \mathbf{C}_H using (G.5)
 - 23: **Option B: Subarray-level Fusion**
 - 24: **for** each subarray pair (m, n) **do**
 - 25: Compute local estimates $\mathbf{m}_p^{(mn)}, \mathbf{C}_p^{(mn)}$ using (50)
 - 26: **end for**
 - 27: Fuse local estimates $\mathbf{m}_p^{(mn)}, \mathbf{C}_p^{(mn)}$ to obtain $\hat{\mathbf{p}}_0, \mathbf{C}_G$ using (51)
 - 28: **for** each subarray pair configuration $\omega_i \in \Omega$ **do**
 - 29: Compute local estimates $\mathbf{m}_v^{(\omega_i)}, \mathbf{C}_v^{(\omega_i)}$ using (57)
 - 30: **end for**
 - 31: Fuse local estimates $\mathbf{m}_v^{(\omega_i)}, \mathbf{C}_v^{(\omega_i)}$ to obtain $\hat{\mathbf{v}}_0, \mathbf{C}_H$ using (58)
-

However, direct computation of \mathbf{F} is challenging due to the nonlinear coupling between $\boldsymbol{\eta}$ and the physical observation model. To address this, we first derive the FIM for the intermediate parameters $\boldsymbol{\rho}$, followed by a transformation via the chain rule.

The FIM for $\boldsymbol{\rho}$ is formulated as:

$$\mathbf{F}_{\boldsymbol{\rho}} = \frac{2}{\sigma} \sum_{m=1}^{K_t} \sum_{n=1}^{K_r} \sum_{l=0}^{L-1} \Re \left\{ \left(\frac{\partial(\beta_{mn} \boldsymbol{\mu}_{mn}^{(l)})}{\partial \boldsymbol{\rho}} \right)^H \left(\frac{\partial(\beta_{mn} \boldsymbol{\mu}_{mn}^{(l)})}{\partial \boldsymbol{\rho}} \right) \right\}. \quad (61)$$

Then, by using the Jacobian matrix $\boldsymbol{\Psi} \triangleq \frac{\partial \boldsymbol{\rho}}{\partial \boldsymbol{\eta}}$ and the chain rule $\frac{\partial(\beta_{mn} \boldsymbol{\mu}_{mn}^{(l)})}{\partial \boldsymbol{\eta}} = \frac{\partial(\beta_{mn} \boldsymbol{\mu}_{mn}^{(l)})}{\partial \boldsymbol{\rho}} \boldsymbol{\Psi}$, the FIM for $\boldsymbol{\eta}$ can be obtained through the transformation:

$$\mathbf{F}_{\boldsymbol{\eta}} = \boldsymbol{\Psi}^T \mathbf{F}_{\boldsymbol{\rho}} \boldsymbol{\Psi}. \quad (62)$$

The calculations for the terms in $\frac{\partial(\beta_{mn} \boldsymbol{\mu}_{mn}^{(l)})}{\partial \boldsymbol{\rho}}$ and $\boldsymbol{\Psi}$ are derived as following. The nonzero entries of $\frac{\partial(\beta_{mn} \boldsymbol{\mu}_{mn}^{(l)})}{\partial \boldsymbol{\rho}}$ are calculated by

$$\frac{\partial(\beta_{mn} \boldsymbol{\mu}_{mn}^{(l)})}{\partial \Re\{\beta_{mn}\}} = \boldsymbol{\mu}_{mn}^{(l)}, \quad \frac{\partial(\beta_{mn} \boldsymbol{\mu}_{mn}^{(l)})}{\partial \Im\{\beta_{mn}\}} = j \boldsymbol{\mu}_{mn}^{(l)}, \quad (63)$$

$$\begin{aligned} \frac{\partial(\beta_{mn} \boldsymbol{\mu}_{mn}^{(l)})}{\partial \theta_m} &= j \beta_{mn} [e^{-j2\pi f_{mn} t_l} \mathbf{a}_r(\phi_n) \otimes (\mathbf{c} \odot \mathbf{a}_t(\theta_m))] \\ &+ 2\pi t_l / \lambda e^{-j2\pi f_{mn} t_l} (\tan(\tilde{\theta}_m) v_x - v_y) \mathbf{a}_r(\phi_n) \otimes \mathbf{a}_t(\theta_m), \end{aligned} \quad (64)$$

where $\mathbf{c} \triangleq [0, 1, \dots, M-1]^T$. Similarly, we have

$$\begin{aligned} \frac{\partial(\beta_{mn} \boldsymbol{\mu}_{mn}^{(l)})}{\partial \phi_n} &= j \beta_{mn} [e^{-j2\pi f_{mn} t_l} (\mathbf{c} \odot \mathbf{a}_r(\phi_n)) \otimes \mathbf{a}_t(\theta_m)] \\ &+ 2\pi t_l / \lambda e^{-j2\pi f_{mn} t_l} (\tan(\tilde{\phi}_n) v_x - v_y) \mathbf{a}_r(\phi_n) \otimes \mathbf{a}_t(\theta_m), \end{aligned} \quad (65)$$

$$\begin{aligned} \frac{\partial(\beta_{mn} \boldsymbol{\mu}_{mn}^{(l)})}{\partial f_{mn}} &= j \beta_{mn} e^{-j2\pi f_{mn} t_l} \left[\frac{\lambda (\mathbf{c} \odot \mathbf{a}_r(\phi_n))}{v_y - \tan(\tilde{\phi}_n) v_x} \otimes \mathbf{a}_t(\theta_m) \right. \\ &\left. - 2\pi t_l \mathbf{a}_r(\phi_n) \otimes \mathbf{a}_t(\theta_m) + \mathbf{a}_r(\phi_n) \otimes \frac{\lambda (\mathbf{c} \odot \mathbf{a}_t(\theta_m))}{v_y - \tan(\tilde{\theta}_m) v_x} \right]. \end{aligned} \quad (66)$$

The nonzero entries in $\boldsymbol{\Psi}$ are calculated based on (14) given by

$$\frac{\partial \theta_m}{\partial \mathbf{p}_0} = \frac{\partial(\mathbf{e}_m^t)^T \mathbf{e}_x}{\partial \mathbf{p}_0} = \frac{-\mathbf{e}_x + (\mathbf{e}_m^t)^T \mathbf{e}_x (\mathbf{e}_m^t)^T}{\|\mathbf{p}_m^t - \mathbf{p}_0\|_2}, \quad (67)$$

$$\frac{\partial \phi_n}{\partial \mathbf{p}_0} = \frac{\partial(\mathbf{e}_n^r)^T \mathbf{e}_x}{\partial \mathbf{p}_0} = \frac{-\mathbf{e}_x + (\mathbf{e}_n^r)^T \mathbf{e}_x (\mathbf{e}_n^r)^T}{\|\mathbf{p}_n^r - \mathbf{p}_0\|_2}, \quad (68)$$

$$\frac{\partial f_{mn}}{\partial \mathbf{p}_0} = \frac{-\mathbf{v}_0 + (\mathbf{e}_m^t)^T \mathbf{v}_0 (\mathbf{e}_m^t)^T}{\|\mathbf{p}_m^t - \mathbf{p}_0\|_2} + \frac{-\mathbf{v}_0 + (\mathbf{e}_n^r)^T \mathbf{v}_0 (\mathbf{e}_n^r)^T}{\|\mathbf{p}_n^r - \mathbf{p}_0\|_2}, \quad (69)$$

$$\frac{\partial f_{mn}}{\partial \mathbf{v}_0} = \mathbf{e}_m^t + \mathbf{e}_n^r, \quad \frac{\partial \Re\{\beta_{mn}\}}{\partial \Re\{\beta_{mn}\}} = 1, \quad \frac{\partial \Im\{\beta_{mn}\}}{\partial \Im\{\beta_{mn}\}} = 1. \quad (70)$$

VII. NUMERICAL SIMULATION

In this section, we presents a comprehensive performance evaluation of the proposed VMP-NMPE algorithm through numerical simulations. We compare our method against three benchmarks:

- 1) **Maximum Likelihood Estimation** (labeled ‘‘ML Estimation’’): This scheme jointly estimates the target location \mathbf{p}_0 , velocity \mathbf{v}_0 , and complex amplitudes $\boldsymbol{\beta}$ by solving the optimization problem [17]:

$$\min_{\mathbf{p}_0, \mathbf{v}_0, \boldsymbol{\beta}} \sum_{m=1}^{K_t} \sum_{n=1}^{K_r} \|\mathbf{z}_{mn} - \beta_{mn} \boldsymbol{\mu}_{mn}(\mathbf{p}_0, \mathbf{v}_0)\|_2^2 \quad (71)$$

The gradient descent algorithm is employed to solve this problem and obtain the ML estimates of \mathbf{p}_0 and \mathbf{v}_0 .

- 2) **Grid-based Method**: This is a two-stage algorithm that first estimates the location using a grid search approach. Then, it employs the 2D MUSIC algorithm to estimate the velocity based on the estimated location.
- 3) **Subarray-level Average**: In this scheme, each T-R subarray pair independently estimates the location and velocity. These subarray-level estimates are then averaged to obtain the final location and velocity estimates.

TABLE II
RADAR SETTINGS USED IN THE SIMULATIONS

Parameter	Value	Parameter	Value
P_T	30 dBm	σ	1 m ²
T	10 μ s	L	600
B	200 MHz	f_c	28 GHz
G_T/G_R	15 dB	N_t/N_r	256
\mathbf{p}_0	(15,20.7) m	\mathbf{v}_0	(10,10.2) m/s

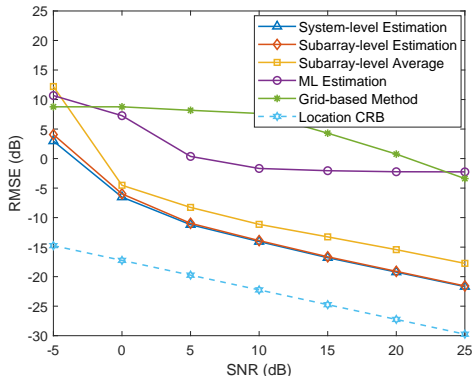


Fig. 4. RMSE of location estimation for the proposed algorithms compared with benchmark schemes versus receive SNR.

The system configuration parameters are detailed in Table II. We quantify the estimation performance using the root mean square error (RMSE) metrics for both location and velocity:

$$\text{RMSE}(\mathbf{p}_0) \triangleq \sqrt{\mathbb{E}(|\hat{x}_0 - x_0|^2 + |\hat{y}_0 - y_0|^2)}, \quad (72a)$$

$$\text{RMSE}(\mathbf{v}_0) \triangleq \sqrt{\mathbb{E}(|\hat{v}_x - v_x|^2 + |\hat{v}_y - v_y|^2)}. \quad (72b)$$

The derived CRBs are served as theoretical performance benchmarks for both location and velocity estimation. All numerical results are statistically validated through 200 independent Monte Carlo trials.

Fig. 4 compares the localization accuracy of the proposed system-level and subarray-level algorithms with three benchmark schemes. Both proposed algorithms demonstrate superior performance over all baselines across the entire SNR range, achieving comparable estimation errors that asymptotically approach the CRB at high SNRs. The performance improvement originates from an adaptive reliability weighting mechanism governed by concentration parameters $\kappa_{\theta_m \rightarrow p_{\theta_m}}$ and $\kappa_{\phi_n \rightarrow p_{\phi_n}}$ in (39) and (41), which effectively suppresses low-quality subarray measurements. This contrasts with the subarray-averaging scheme that naively combines estimates with equal weights, thereby amplifying noise impacts particularly at low-to-moderate SNRs. The system-level approach marginally outperforms the subarray-level counterpart by exploiting cross-subarray information. Compared to conventional approaches, our variational framework fundamentally overcomes following limitations: 1) The ML Estimation suffers from local minima in high-dimensional optimization; 2) Grid search method suffer from discretization errors and cascaded error propagation, whereas the proposed methods leverage VBI to provide continuous domain modeling, thereby eliminating

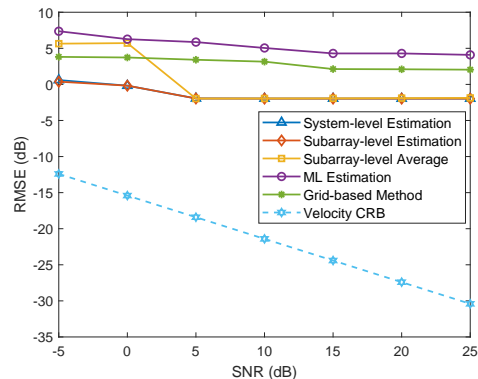


Fig. 5. RMSE of velocity estimation for the proposed algorithms compared with benchmark schemes versus receive SNR.

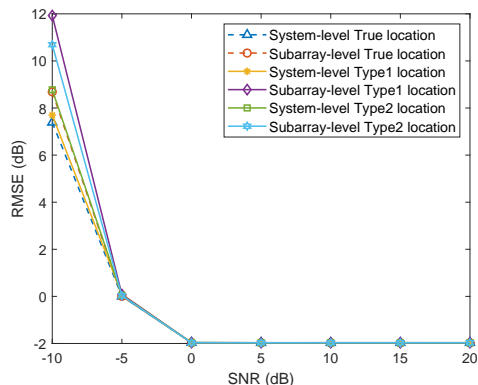


Fig. 6. Impact of location estimation accuracy on velocity estimation performance.

grid mismatches and enhancing estimation accuracy. These advantages are particularly pronounced in challenging low-SNR scenarios where the proposed reliability-aware fusion strategies demonstrate robust noise suppression capabilities.

Fig. 5 compares the velocity estimation performance of the proposed system-level and subarray-level algorithms with three benchmark schemes. Both system-level and subarray-level variants achieve comparable performance, consistently outperforming all baselines. The ML Estimator exhibits the worst accuracy due to its requirement for joint optimization over coupled position-velocity parameters, which creates complex local optima in high-dimensional space. The grid-based method shows discretization-induced error floor, which can be mitigated through our continuous parameter space modeling via VBI. As the SNR increases, the performance gaps between subarray-averaging and proposed methods narrows. This occurs because high-SNR conditions render subarray measurements sufficiently reliable for naive averaging. However, a discrepancy remains between these converged RMSE values and the CRB for velocity estimation. This may originate from theoretical constraints of variational approximation, while the mean-field assumption enables tractable inference, it introduces minor information loss in modeling parameter correlations.

Fig. 6 demonstrates the impact of location estimation accuracy on velocity estimation, where "True" uses the actual

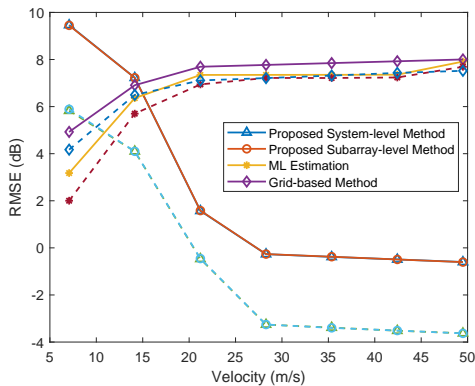


Fig. 7. Impact of target mobility on velocity estimation performance at SNR = 0dB.

location, while "Type 1" and "Type 2" employ system-level and subarray-level estimated locations, respectively. At low SNRs, the subarray-level method's velocity estimation suffers considerably, and the choice of location estimation method (True, Type 1, or Type 2) significantly affects the results. This degradation stems from error amplification through the bistatic Doppler coupling in (14c), causing biased gradient calculations in velocity estimation. In contrast, the proposed system-level method can closely match the performance achieved when using the true location, regardless of the location estimation type (Type 1 or Type 2). This is due to the system-level approach's ability to coherently fuse information from all subarray pairs, mitigating the impact of individual subarray estimation errors. As SNR increases, all methods converge to similarly low RMSE values, validating the asymptotic optimality of our approach.

Fig. 7 illustrates the impact of target mobility on the velocity estimation performance at an SNR of 0 dB for CPI lengths $L = 400$ (solid lines) and $L = 800$ (dashed lines). In these simulations, the target's location and velocity direction remain constant, while the velocity magnitude varies. It is observed that the extended CPI operation enhances the precision of velocity estimation, and the performance gap between the proposed and conventional methods progressively increases with velocity, revealing the inherent advantage of our architecture in high-dynamic scenarios. This velocity resilience stems from two aspects: the high-velocity target induce stronger Doppler diversity across spatially distributed subarrays, creating distinctive frequency signatures that our variational framework effectively decouples and exploits, and the hierarchical message passing architecture inherently compensates for spatial-Doppler coupling through adaptive reliability weighting of subarray measurements.

Fig. 8 illustrates the average running time comparison between the proposed algorithms and benchmark schemes across different SNRs. The computational complexities are $\mathcal{O}(N_{vi}K_tK_rM(M+L))$ for both system-level and subarray-level proposed algorithms, $\mathcal{O}(N_{iter}K_t^2K_r^2M^3L^3)$ for ML estimation, and $\mathcal{O}(K_tK_r(M^6L^3))$ for the grid-based method, where I denotes the number of grid points per parameter dimension. The proposed algorithms achieve 10^{-1} - 10^0 seconds

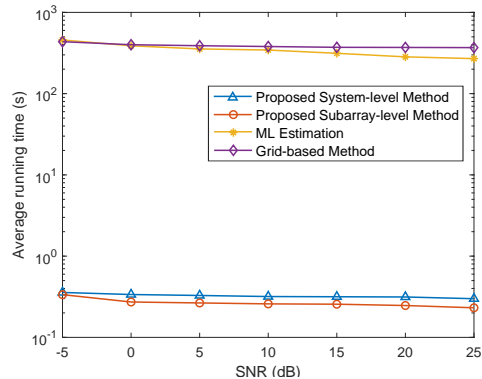


Fig. 8. Average running times for the proposed algorithms compared with benchmark schemes versus receive SNR.

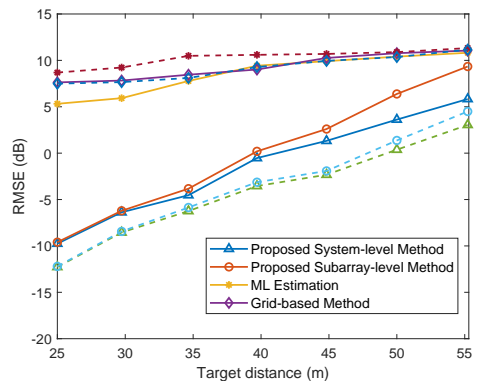


Fig. 9. Impact of target distance on location estimation performance with $M = 32$ and $M = 64$.

average running times, substantially outperforming the ML estimation and the grid-based method (10^2 - 10^3 seconds). This superior efficiency can be attributed to two key factors: the parallel processing capability during the variational inference stage, where parameter estimation for each subarray pair can be computed simultaneously, and the well-structured computational framework that avoids the exponential complexity of grid search and the quadratic dependency on array dimensions of ML estimation.

Fig. 9 illustrates the RMSE of location estimation for subarray sizes $M = 32$ (solid lines) and $M = 64$ (dashed lines), with fixed velocity and total number of transmit and receive antennas. It can be observed that the accuracy of location estimation for all schemes decreases as the distance increases, which is due to the diminishing curvature of the spherical wavefront as the target located farther away from the BS. The performance gap between the benchmark schemes and the proposed methods diminishes with increasing distance due to the gradual weakening of the near-field effect, as the signal propagation becomes more similar to the far-field case. For the two proposed approaches, the location estimation performance with $M = 64$ is consistently better than that with $M = 32$ for each method across all distances. This improvement can be attributed to the more accurate estimation of the DoA and DoD by larger subarrays, which provide a higher angular resolution and are less sensitive to noise, leading to more precise location

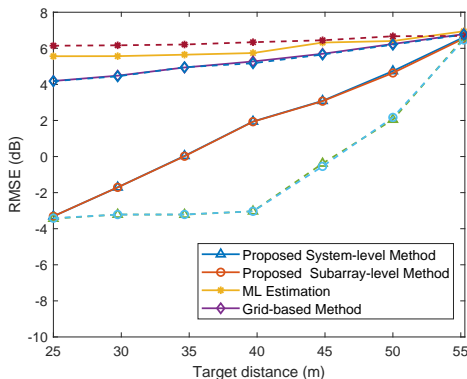


Fig. 10. RMSE of location estimation for the proposed algorithms compared with benchmark schemes versus receive SNR.

estimates after fusion.

Fig. 10 illustrates the RMSE performance of velocity estimation versus target distance for the proposed algorithms and benchmark schemes for subarray sizes $M = 32$ (solid lines) and $M = 64$ (dashed lines). It can be seen that the proposed system-level and subarray-level methods exhibit similar performance across the distance range considered, outperforming the ML estimation and grid-based method. As the target distance increases, the performance gap between the proposed algorithms and the benchmarks diminishes. Similar to Fig. 7, the velocity estimation accuracy improves when $M = 64$ compared to $M = 32$, due to the alternating optimization of Doppler, DoD, and DoA for each subarray during the variational inference process. Larger subarrays enable higher angular estimation precision, which consequently improves the Doppler estimation accuracy.

VIII. CONCLUSION

In this paper, a novel subarray-based VMP algorithm has been proposed for joint near-field location and velocity estimation. Simulation results have demonstrated its superior performance compared to existing methods, achieving centimeter-level location accuracy and sub-m/s velocity accuracy with significantly reduced computational complexity. It has been found that increasing the CPI length or subarray size generally leads to improved estimation accuracy. Moreover, the proposed method has exhibited robust performance for the target with high mobility. Therefore, the low complexity and real-time capability of the proposed algorithm make it highly suitable for implementation in real-world near-field sensing scenarios.

APPENDIX A PROOF OF LEMMA 1

By substituting the joint PDF (17) and postulated PDF (18) into (20), we obtain

$$\ln q(\phi_n | \mathbf{z}_{mn}) = E_{\phi_n} [\ln p(\mathbf{z}_{mn} | \Theta; \alpha)] + \ln p(\phi_n) + \text{const.} \quad (\text{A.1})$$

By substituting the likelihood PDF (10) into (A.1) and retaining only the terms dependent on ϕ_n , we further obtain

$$\ln q(\phi_n | \mathbf{z}_{mn}) = -2/\sigma E_{\phi_n} [\Re\{\mathbf{z}_{mn}^H (\mathbf{a}(\phi_n) \otimes \mathbf{c}_{mn})\}] + \ln p(\phi_n) + \text{const.} \quad (\text{A.2})$$

By carrying out the required expectations, we finally obtain

$$q(\phi_n | \mathbf{z}_{mn}) \propto p(\phi_n) \exp\{\Re((\boldsymbol{\eta}_{mn})^H (\mathbf{a}(\phi_n) \otimes \hat{\mathbf{c}}_{mn}))\}. \quad (\text{A.3})$$

Expressing $\mathbf{a}(\phi_n)$ in terms of the antenna indices, we can rewrite (A.3) as

$$q(\phi_n | \mathbf{z}_{mn}) \propto p(\phi_n) \prod_{k=0}^{M-1} \exp\{\Re(\tilde{\eta}_{\phi_n, k}^* e^{jk\phi_n})\}, \quad (\text{A.4})$$

where $\tilde{\eta}_{\phi_n, k}^* \triangleq [\boldsymbol{\eta}_{mn}]_{kML:(k+1)ML}^H \hat{\mathbf{c}}_{mn}$, which has the polar form $\tilde{\eta}_{\phi_n, k}^* = \kappa_{\phi_n, k} e^{j\mu_{\phi_n, k}}$. When $k = 0$, the corresponding factor in (A.4) is a constant and can be removed. The factors with index $k \geq 1$ have the form of a k -fold wrapped VM distribution $\mathcal{M}(k\phi_n, \tilde{\eta}_{\phi_n, k})$, which can be approximated by a mixture of VM distributions [28].

To fully exploit the multiplicative closure property of VM distributions, we also model the prior distribution of ϕ_n using a VM distribution, i.e., $p(\phi_n) = \mathcal{M}(\phi_n; \bar{\eta}_{\phi_n})$. We define the function to represent the exponent of (A.3), which is given by

$$g(\phi_n) = \Re(\bar{\eta}_{\phi_n}^* e^{j\phi_n}) + \sum_{k=1}^{M-1} \eta_{\phi_n, k}^* e^{jk\phi_n}. \quad (\text{A.5})$$

According to the properties of wrapped normal distributions and their similarity to VM distributions [30], we can obtain the VM approximation of $q(\phi_n | \mathbf{z}_{mn})$ as $\mathcal{M}(\phi_n, \hat{\eta}_{\phi_n})$, where $\hat{\eta}_{\phi_n} = \hat{\kappa}_{\phi_n} e^{j\hat{\phi}_n}$. The mean direction is $\hat{\phi}_n = \bar{\phi}_n - \frac{g'(\phi_n)}{g''(\phi_n)}$, where $\bar{\phi}_n$ is obtained at the maximum of $g(\phi_n)$. The concentration is given by $\hat{\kappa}_{\phi_n} = A^{-1}(\exp(\frac{1}{2g''(\phi_n)}))$, which completes the proof.

APPENDIX B PROOF OF LEMMA 3

Similar to the calculation of $q(\theta_m | \mathbf{z}_{mn})$, maximizing \mathcal{L} w.r.t. $q(f_{mn} | \mathbf{z}_{mn})$ gives

$$q(f_{mn} | \mathbf{z}_{mn}) \propto p(f_{mn}) \exp\{\Re((\mathbf{d}(f_{mn}) \otimes \hat{\mathbf{c}}_{mn}^{(2)})^H (\boldsymbol{\eta}_{mn}^{(2)}))\}, \quad (\text{B.1})$$

where the estimates of $\hat{\phi}_n$ and $\hat{\theta}_m$ are obtained from Lemma 1 and Lemma 2, respectively. Then, we can rewrite (B.1) as

$$q(\tilde{f}_{mn} | \mathbf{z}_{mn}) \propto p(\tilde{f}_{mn}) \prod_{l=1}^{L-1} \exp\{\Re(\tilde{\eta}_{f_{mn}, l}^* e^{j\tilde{f}_{mn}})\}, \quad (\text{B.2})$$

where $\tilde{\eta}_{f_{mn}, l}^* \triangleq (\hat{\mathbf{c}}_{mn}^{(2)})^H [\boldsymbol{\eta}_{mn}^{(2)}]_{lM^2:(l+1)M^2}$, which has the polar form $\tilde{\eta}_{f_{mn}, l}^* = \kappa_{f_{mn}, l} e^{j\mu_{f_{mn}, l}}$.

By approximating the prior distribution with a VM distribution $p(\tilde{f}_{mn}) = \mathcal{M}(\tilde{f}_{mn}; \bar{\eta}_{f_{mn}})$, the exponential term in (B.1) can be represented by the function $g(f_{mn}) = \Re(\bar{\eta}_{f_{mn}}^* e^{j\tilde{f}_{mn}} + \sum_{l=1}^{L-1} \eta_{f_{mn}, l}^* e^{j\tilde{f}_{mn}})$. Consequently, the posterior distribution $q(\tilde{f}_{mn} | \mathbf{z}_{mn})$ can be approximated by a VM distribution $p(\tilde{f}_{mn}) = \mathcal{M}(\tilde{f}_{mn}; \hat{\eta}_{f_{mn}})$, which completes the proof.

APPENDIX C PROOF OF LEMMA 4

The optimal form of $q(\beta_{mn} | \mathbf{z}_{mn})$ can be obtained as

$$\ln q(\beta_{mn} | \mathbf{z}_{mn}) = E_{\beta_{mn}} [\ln p(\mathbf{z}_{mn} | \Theta; \alpha)] + \ln p(\beta_{mn}) + \text{const.} \quad (\text{C.1})$$

By substituting the likelihood PDF (10) into (C.1) and retaining only the terms dependent on β_{mn} , we further obtain

$$q(\beta_{mn}|\mathbf{z}_{mn}) \propto p(\beta_{mn}) \times \exp\{-2/\sigma(2\Re(\beta_{mn}\boldsymbol{\mu}_{mn}^H\mathbf{z}_{mn}) + |\beta_{mn}|^2\|\boldsymbol{\mu}_{mn}\|_2^2)\}. \quad (\text{C.2})$$

Then, we substitute the prior distribution $p(\beta_{mn}) = \mathcal{CN}(0, \varsigma_{mn})$ into (C.2) and completing the square with respect to β_{mn} , we obtain

$$q(\beta_{mn}|\mathbf{z}_{mn}) \propto \exp\{-2/(\varsigma_{mn} + 2/\sigma\|\boldsymbol{\mu}_{mn}\|_2^2)|\beta_{mn}|^2 - 4/\sigma\Re(\beta_{mn}\boldsymbol{\mu}_{mn}^H\mathbf{z}_{mn})\}. \quad (\text{C.3})$$

Therefore, we obtain $q(\beta_{mn}|\mathbf{z}_{mn}) \propto \mathcal{CN}(\hat{\beta}_{mn}, \tilde{\varsigma}_{mn})$, where the mean and variance of the Gaussian posterior PDF of β_{mn} are

$$\hat{\beta}_{mn} = \frac{\varsigma_{mn}\boldsymbol{\mu}_{mn}^H\mathbf{z}_{mn}}{\sigma + \varsigma_{mn}\|\boldsymbol{\mu}_{mn}\|_2^2}, \quad \tilde{\varsigma}_{mn} = \frac{\varsigma_{mn}\sigma}{2(\sigma + \varsigma_{mn}\|\boldsymbol{\mu}_{mn}\|_2^2)}, \quad (\text{C.4})$$

which completes the proof.

APPENDIX D PROOF OF LEMMA 5

With the factorized variational distributions $q(\Theta|\mathbf{z}_{mn})$ fixed, the ELBO \mathcal{L} in (19) can be expressed as a function of the hyperparameters α , which is given by

$$\mathcal{L}(\alpha) = E_{q(\Theta|\mathbf{z}_{mn})}[\ln p(\mathbf{z}_{mn}|\Theta; \alpha) + \ln p(\beta_{mn}; \alpha)] + \text{const}. \quad (\text{D.1})$$

Substituting the likelihood PDF (10) and the prior distribution of β_{mn} into (D.1) and take the corresponding expectations, we obtain

$$\mathcal{L}(\alpha) = -M^2L \ln \sigma - \ln \varsigma_{mn} - 2/\varsigma_{mn}(\tilde{\varsigma}_{mn} + |\hat{\beta}_{mn}|^2) - 2/\sigma(\|\mathbf{z}_{mn}\|_2^2 + 2\Re(\hat{\beta}_{mn}\boldsymbol{\mu}_{mn}^H\hat{\boldsymbol{\mu}}_{mn}) + \|\hat{\boldsymbol{\mu}}_{mn}\|_2^2(\tilde{\varsigma}_{mn} + |\hat{\beta}_{mn}|^2)), \quad (\text{D.2})$$

where the derivation is based on the fact that $E_{q(\beta_{mn}|\mathbf{z}_{mn})}[\beta_{mn}] = \hat{\beta}_{mn}$, and $E_{q(\beta_{mn}|\mathbf{z}_{mn})}[|\beta_{mn}|^2] = \tilde{\varsigma}_{mn} + |\hat{\beta}_{mn}|^2$.

To obtain the estimates of the hyperparameters, we take the partial derivatives of $\mathcal{L}(\alpha)$ with respect to σ and ς_{mn} , respectively. By setting the partial derivatives to zero and solving the resulting equations, we obtain the closed-form expressions for the hyperparameter estimates in (34), which completes the proof.

APPENDIX E GAUSSIAN MESSAGE APPROXIMATION IN (48)

The expression of $\prod_{m=1}^{K_t} \prod_{n=1}^{K_r} \Delta_{p_{\theta_m} \rightarrow \mathbf{p}_0}(\mathbf{p}_0) \Delta_{p_{\phi_n} \rightarrow \mathbf{p}_0}(\mathbf{p}_0)$ is given by

$$\prod_{m=1}^{K_t} \prod_{n=1}^{K_r} \Delta_{p_{\theta_m} \rightarrow \mathbf{p}_0}(\mathbf{p}_0) \Delta_{p_{\phi_n} \rightarrow \mathbf{p}_0}(\mathbf{p}_0) \propto \exp\left\{\sum_{m=1}^{K_t} \sum_{n=1}^{K_r} \kappa_{\theta_m \rightarrow p_{\theta_m}} \cos(\chi(\mathbf{e}_m^t)^T \mathbf{e}_x - \mu_{\theta_m \rightarrow p_{\theta_m}}) + \kappa_{\phi_n \rightarrow p_{\phi_n}} \cos(\chi(\mathbf{e}_n^r)^T \mathbf{e}_x - \mu_{\phi_n \rightarrow p_{\phi_n}})\right\}, \quad (\text{E.1})$$

where $\chi \triangleq \frac{2\pi d}{\lambda}$, $\mathbf{e}_m^t \triangleq \frac{\mathbf{p}_0 - \mathbf{p}_m^t}{\|\mathbf{p}_0 - \mathbf{p}_m^t\|_2}$, and $\mathbf{e}_n^r \triangleq \frac{\mathbf{p}_0 - \mathbf{p}_n^r}{\|\mathbf{p}_0 - \mathbf{p}_n^r\|_2}$.

We resort to the gradient descent method to find the local maximum of (E.1) which is used as the mean vector \mathbf{m}_G of

the approximated Gaussian message in (48). The covariance matrix \mathbf{C}_G of the approximated Gaussian message is given by the Hessian matrix at $\mathbf{p}_0 = \mathbf{m}_G$. We denote the exponential term of (E.1) as $f_p(\mathbf{p}_0)$. Thus, the gradient of $f_p(\mathbf{p}_0)$ is derived as

$$\frac{\partial f_p(\mathbf{p}_0)}{\partial \mathbf{p}_0} = \sum_{m=1}^{K_t} \sum_{n=1}^{K_r} \boldsymbol{\vartheta}_m^t + \boldsymbol{\vartheta}_n^r, \quad (\text{E.2})$$

with

$$\boldsymbol{\vartheta}_m^t \triangleq -\chi \kappa_{\theta_m \rightarrow p_{\theta_m}} \sin(\chi(\mathbf{e}_m^t)^T \mathbf{e}_x - \mu_{\theta_m \rightarrow p_{\theta_m}}) \mathbf{w}_m^t, \quad (\text{E.3})$$

$$\boldsymbol{\vartheta}_n^r \triangleq -\chi \kappa_{\phi_n \rightarrow p_{\phi_n}} \sin(\chi(\mathbf{e}_n^r)^T \mathbf{e}_x - \mu_{\phi_n \rightarrow p_{\phi_n}}) \mathbf{w}_n^r,$$

where

$$\mathbf{w}_m^t \triangleq \frac{\partial(\mathbf{e}_m^t)^T \mathbf{e}_x}{\partial \mathbf{p}_0} = \frac{-\mathbf{e}_x + (\mathbf{e}_m^t)^T \mathbf{e}_x \mathbf{e}_m^t}{\|\mathbf{p}_m^t - \mathbf{p}_0\|_2}, \quad (\text{E.4})$$

$$\mathbf{w}_n^r \triangleq \frac{\partial(\mathbf{e}_n^r)^T \mathbf{e}_x}{\partial \mathbf{p}_0} = \frac{-\mathbf{e}_x + (\mathbf{e}_n^r)^T \mathbf{e}_x \mathbf{e}_n^r}{\|\mathbf{p}_n^r - \mathbf{p}_0\|_2}.$$

Therefore, we iteratively update \mathbf{p}_0 according to the following rule:

$$\mathbf{p}_0^{(i+1)} = \mathbf{p}_0^{(i)} + \delta_p \left. \frac{\partial f_p(\mathbf{p}_0)}{\partial \mathbf{p}_0} \right|_{\mathbf{p}_0 = \mathbf{p}_0^{(i)}}, \quad (\text{E.5})$$

where δ_p is the step size and i is the iteration index. The iteration stops when \mathbf{p}_0 reaches a local optimum, which is obtained as \mathbf{m}_G .

The covariance matrix \mathbf{C}_G is obtained by calculating the Hessian matrix of $f_p(\mathbf{p}_0)$ at \mathbf{m}_G . The Hessian matrix of $f_p(\mathbf{p}_0)$ is obtained as

$$\frac{\partial^2 f_p(\mathbf{p}_0)}{\partial \mathbf{p}_0 \partial \mathbf{p}_0^T} = \sum_{m=1}^{K_t} \sum_{n=1}^{K_r} \mathbf{J}_m^t + \mathbf{J}_n^r, \quad (\text{E.6})$$

with

$$\mathbf{J}_m^t = -\chi^2 \kappa_{\theta_m \rightarrow p_{\theta_m}} \cos(\chi(\mathbf{e}_m^t)^T \mathbf{e}_x - \mu_{\theta_m \rightarrow p_{\theta_m}}) \mathbf{w}_m^t (\mathbf{w}_m^t)^T - \chi \kappa_{\theta_m \rightarrow p_{\theta_m}} \sin(\chi(\mathbf{e}_m^t)^T \mathbf{e}_x - \mu_{\theta_m \rightarrow p_{\theta_m}}) \frac{\partial \mathbf{w}_m^t}{\partial \mathbf{p}_0^T}, \quad (\text{E.7})$$

where

$$\frac{\partial \mathbf{w}_m^t}{\partial \mathbf{p}_0^T} = \frac{-2\mathbf{e}_x(\mathbf{e}_m^t)^T + 3(\mathbf{e}_m^t)^T \mathbf{e}_x \mathbf{e}_m^t (\mathbf{e}_m^t)^T - (\mathbf{e}_m^t)^T \mathbf{e}_x \mathbf{I}}{\|\mathbf{p}_m^t - \mathbf{p}_0\|_2}. \quad (\text{E.8})$$

The matrix \mathbf{J}_n^r can be calculated similarly.

Therefore, the covariance matrix \mathbf{C}_G is obtained as the negative inverse of the Hessian matrix of $f_p(\mathbf{p}_0)$ at \mathbf{m}_G , which is given by

$$\mathbf{C}_G^{-1} = - \left. \frac{\partial^2 f_p(\mathbf{p}_0)}{\partial \mathbf{p}_0 \partial \mathbf{p}_0^T} \right|_{\mathbf{p}_0 = \mathbf{m}_G}. \quad (\text{E.9})$$

APPENDIX F GAUSSIAN MESSAGE APPROXIMATION IN (50)

Based on (E.1), the condition for the function $\ln(\Delta_{p_{\theta_m} \rightarrow \mathbf{p}_0}(\mathbf{p}_0) \Delta_{p_{\phi_n} \rightarrow \mathbf{p}_0}(\mathbf{p}_0))$ to reach its maximum value is:

$$\sin \tilde{\theta}_m = \frac{\mu_{\theta_m \rightarrow p_{\theta_m}}}{\chi}, \quad \sin \tilde{\phi}_n = \frac{\mu_{\phi_n \rightarrow p_{\phi_n}}}{\chi}. \quad (\text{F.1})$$

Therefore, we have $\mathbf{e}_m^t = \left[\frac{1}{\chi} \mu_{\theta_m \rightarrow p_{\theta_m}}, \sqrt{1 - \frac{1}{\chi^2} \mu_{\theta_m \rightarrow p_{\theta_m}}^2} \right]$, and $\mathbf{e}_n^r = \left[\frac{1}{\chi} \mu_{\phi_n \rightarrow p_{\phi_n}}, \sqrt{1 - \frac{1}{\chi^2} \mu_{\phi_n \rightarrow p_{\phi_n}}^2} \right]$.

By denoting the distances $\|\mathbf{p}_n^r - \mathbf{p}_0\|_2$ and $\|\mathbf{p}_m^t - \mathbf{p}_0\|_2$ as d_n^r and d_m^t , respectively, we can obtain the bistatic range for (m, n) -th T-R subarray pair as $d_n^r + d_m^t = c\hat{\tau}_{mn}$, where $\hat{\tau}_{mn}$ is the estimated bistatic time delay derived from the previous matched filtering step. Therefore, the maximum can be obtained as $\mathbf{m}_p^{(mn)} = \mathbf{p}_n^r - d_n^r \mathbf{e}_n^r = \mathbf{p}_m^t - d_m^t \mathbf{e}_m^t$, where the bistatic ranges are given by $d_n^r = \frac{c\hat{\tau}_{mn} \sqrt{1 - \mu_{\theta_m \rightarrow p_{\theta_m}}^2 / \chi^2}}{\sqrt{1 - \mu_{\theta_m \rightarrow p_{\theta_m}}^2 / \chi^2} + \sqrt{1 - \mu_{\phi_n \rightarrow p_{\phi_n}}^2 / \chi^2}}$ and $d_m^t = \frac{c\hat{\tau}_{mn} \sqrt{1 - \mu_{\phi_n \rightarrow p_{\phi_n}}^2 / \chi^2}}{\sqrt{1 - \mu_{\theta_m \rightarrow p_{\theta_m}}^2 / \chi^2} + \sqrt{1 - \mu_{\phi_n \rightarrow p_{\phi_n}}^2 / \chi^2}}$, respectively.

Based on (E.6), the Hessian matrix of the function $\ln(\Delta_{p_{\theta_m} \rightarrow p_0}(\mathbf{p}_0) \Delta_{p_{\phi_n} \rightarrow p_0}(\mathbf{p}_0))$ is given by $\mathbf{J}_p^{(mn)} = \mathbf{J}_m^t + \mathbf{J}_n^r$. Therefore, the covariance matrix of the Gaussian distribution can be approximated by the inverse of the Hessian matrix evaluated at the maximum point $\mathbf{m}_p^{(mn)}$:

$$\mathbf{C}_p^{(m,n)} \approx -(\mathbf{J}_p^{(mn)})^{-1} \Big|_{\mathbf{p}_0 = \mathbf{m}_p^{(mn)}}, \quad (\text{F.2})$$

with

$$\begin{aligned} \mathbf{J}_p^{(mn)} \Big|_{\mathbf{p}_0 = \mathbf{m}_p^{(mn)}} = & \frac{\chi^2 \kappa_{\theta_m \rightarrow p_{\theta_m}}}{d_m^t} (2\mathbf{e}_x(\mathbf{e}_m^t)^T - 3(\mathbf{e}_m^t)^T \mathbf{e}_x \mathbf{e}_m^t (\mathbf{e}_m^t)^T + (\mathbf{e}_m^t)^T \mathbf{e}_x \mathbf{I}) \\ & + \frac{\chi^2 \kappa_{\phi_n \rightarrow p_{\phi_n}}}{d_n^r} (2\mathbf{e}_x(\mathbf{e}_n^r)^T - 3(\mathbf{e}_n^r)^T \mathbf{e}_x \mathbf{e}_n^r (\mathbf{e}_n^r)^T + (\mathbf{e}_n^r)^T \mathbf{e}_x \mathbf{I}). \end{aligned} \quad (\text{F.3})$$

APPENDIX G

GAUSSIAN MESSAGE APPROXIMATION IN (55)

Based on Definition 1, the expression in (54) can be rewritten as

$$\prod_{m=1}^{K_t} \prod_{n=1}^{K_r} \Delta_{p_{f_{mn}} \rightarrow \mathbf{v}_0}(\mathbf{v}_0) \propto \exp\left\{\sum_{m,n} \kappa_{f_{mn} \rightarrow p_{f_{mn}}} \cos(\zeta \mathbf{v}_0^T \mathbf{u}_{mn} - \mu_{f_{mn} \rightarrow p_{f_{mn}}})\right\}. \quad (\text{G.1})$$

Denoting the exponential term in (G.1) as a function, we have

$$f_v(\mathbf{v}_0) \triangleq \sum_{m,n} \kappa_{f_{mn} \rightarrow p_{f_{mn}}} \cos(\zeta \mathbf{v}_0^T \mathbf{u}_{mn} - \mu_{f_{mn} \rightarrow p_{f_{mn}}}). \quad (\text{G.2})$$

The mean vector $\mathbf{m}_{\mathcal{H}}$ is obtained at the local maximum of $f_v(\mathbf{v}_0)$ using the gradient ascent method:

$$\mathbf{v}_0^{(i+1)} = \mathbf{v}_0^{(i)} + \delta_v \left. \frac{\partial f_v(\mathbf{v}_0)}{\partial \mathbf{v}_0} \right|_{\mathbf{v}_0 = \mathbf{v}_0^{(i)}}, \quad (\text{G.3})$$

where δ_v is the step size, i is the iteration index, and $\frac{\partial f_v(\mathbf{v}_0)}{\partial \mathbf{v}_0}$ denotes the gradient of $f_v(\mathbf{v}_0)$ with respect to \mathbf{v}_0 , which is given by

$$\frac{\partial f_v(\mathbf{v}_0)}{\partial \mathbf{v}_0} = -\sum_{m,n} \zeta \kappa_{f_{mn} \rightarrow p_{f_{mn}}} \sin(\zeta \mathbf{v}_0^T \mathbf{u}_{mn} - \mu_{f_{mn} \rightarrow p_{f_{mn}}}) \mathbf{u}_{mn}. \quad (\text{G.4})$$

The covariance matrix $\mathbf{C}_{\mathcal{H}}$ is obtained as the negative inverse of the Hessian matrix of $f_v(\mathbf{v}_0)$ evaluated at $\mathbf{m}_{\mathcal{H}}$:

$$\mathbf{C}_{\mathcal{H}} = \left(-\left. \frac{\partial f_v(\mathbf{v}_0)}{\partial \mathbf{v}_0 \partial \mathbf{v}_0^T} \right|_{\mathbf{v}_0 = \mathbf{m}_{\mathcal{H}}} \right)^{-1}, \quad (\text{G.5})$$

where

$$\begin{aligned} \frac{\partial f_v(\mathbf{v}_0)}{\partial \mathbf{v}_0 \partial \mathbf{v}_0^T} = & -\sum_{m,n} \zeta^2 \kappa_{f_{mn} \rightarrow p_{f_{mn}}} \times \\ & \cos(\zeta \mathbf{v}_0^T \mathbf{u}_{mn} - \mu_{f_{mn} \rightarrow p_{f_{mn}}}) \mathbf{u}_{mn} \mathbf{u}_{mn}^T. \end{aligned} \quad (\text{G.6})$$

APPENDIX H

GAUSSIAN MESSAGE APPROXIMATION IN (57)

The logarithm of the marginal PDF in (56) can be expressed as

$$\begin{aligned} \Delta_{\mathbf{v}_0}^{(\omega_i)}(\mathbf{v}_0) \propto & \exp\left\{\kappa_{f_{mn} \rightarrow p_{f_{mn}}} \cos(\zeta \mathbf{v}_0^T \mathbf{u}_{mn} - \mu_{f_{mn} \rightarrow p_{f_{mn}}})\right. \\ & \left. + \kappa_{f_{pq} \rightarrow p_{f_{pq}}} \cos(\zeta \mathbf{v}_0^T \mathbf{u}_{pq} - \mu_{f_{pq} \rightarrow p_{f_{pq}}})\right\}. \end{aligned} \quad (\text{H.1})$$

The mean of the Gaussian distribution is obtained at the maximum of $\ln(\Delta_{\mathbf{v}_0}^{(\omega_i)}(\mathbf{v}_0))$, which is achieved when the following equality holds:

$$\mathbf{v}_0^T \mathbf{E}_{\omega_i} = \mu_{\omega_i} / \zeta, \quad (\text{H.2})$$

where we define $\mathbf{E}_{\omega_i} \triangleq [\mathbf{u}_{mn}, \mathbf{u}_{pq}]$ and $\mu_{\omega_i} \triangleq [\mu_{f_{mn} \rightarrow p_{f_{mn}}}, \mu_{f_{pq} \rightarrow p_{f_{pq}}}]^T$.

Therefore, the mean vector is given by

$$\mathbf{m}_v^{(\omega_i)} = (\mathbf{E}_{\omega_i}^T)^{-1} \mu_{\omega_i} / \zeta. \quad (\text{H.3})$$

Based on (G.6), the covariance matrix is given by

$$\mathbf{C}_v^{(\omega_i)} = -(\kappa_{f_{mn} \rightarrow p_{f_{mn}}} \mathbf{u}_{mn} \mathbf{u}_{mn}^T + \kappa_{f_{pq} \rightarrow p_{f_{pq}}} \mathbf{u}_{pq} \mathbf{u}_{pq}^T)^{-1} / \zeta^2. \quad (\text{H.4})$$

REFERENCES

- [1] F. Liu, Y. Cui, C. Masouros, J. Xu, T. X. Han, Y. C. Eldar, and S. Buzzi, "Integrated sensing and communications: Toward dual-functional wireless networks for 6G and beyond," *IEEE J. Sel. Areas Commun.*, vol. 40, no. 6, pp. 1728–1767, Mar. 2022.
- [2] F. Dong, F. Liu, Y. Cui, S. Lu, and Y. Li, "Sensing as a service in 6G perceptible mobile networks: Architecture, advances, and the road ahead," *IEEE Network*, vol. 38, no. 2, pp. 87–96, Mar. 2024.
- [3] Z. Wei, H. Qu, Y. Wang, X. Yuan, H. Wu, Y. Du, K. Han, N. Zhang, and Z. Feng, "Integrated sensing and communication signals toward 5G-A and 6G: A survey," *IEEE Internet Things J.*, vol. 10, no. 13, pp. 11 068–11 092, 2023.
- [4] Y. Liu, Z. Wang, J. Xu, C. Ouyang, X. Mu, and R. Schober, "Near-field communications: A tutorial review," *IEEE Open J. Commun. Soc.*, vol. 4, pp. 1999–2049, Aug. 2023.
- [5] Z. Wang, X. Mu, and Y. Liu, "Near-field integrated sensing and communications," *IEEE Commun. Lett.*, vol. 27, no. 8, pp. 2048–2052, Aug. 2023.
- [6] J. Cong, C. You, J. Li, L. Chen, B. Zheng, Y. Liu, W. Wu, Y. Gong, S. Jin, and R. Zhang, "Near-field integrated sensing and communication: Opportunities and challenges," *IEEE Wirel. Commun.*, pp. 1–8, Sept. 2024.
- [7] Y. Liu, Z. Wang, J. Xu, C. Ouyang, X. Mu, and R. Schober, "Near-field communications: A tutorial review," *IEEE Open J. Commun. Soc.*, vol. 4, pp. 1999–2049, Aug. 2023.
- [8] Z. Wang, J. Zhang, H. Du, D. Niyato, S. Cui, B. Ai, M. Debbah, K. B. Letaief, and H. V. Poor, "A tutorial on extremely large-scale MIMO for 6G: Fundamentals, signal processing, and applications," *IEEE Commun. Surv. Tutor.*, vol. 26, no. 3, pp. 1560–1605, Jan. 2024.
- [9] S. Liu, X. Yu, Z. Gao, J. Xu, D. W. K. Ng, and S. Cui, "Sensing-enhanced channel estimation for near-field XL-MIMO systems," *IEEE J. Sel. Areas Commun.*, pp. 1–1, Jan. 2025.
- [10] Z. Wang, X. Mu, and Y. Liu, "Rethinking integrated sensing and communication: When near field meets wideband," *IEEE Commun. Mag.*, vol. 62, no. 9, pp. 44–50, Sept. 2024.
- [11] S. Yang, W. Lyu, Z. Zhang, and C. Yuen, "Enhancing near-field sensing and communications with sparse arrays: Potentials, challenges, and emerging trends," *arXiv preprint arXiv:2309.08681*, 2023.

- [12] S. Yang, X. Chen, Y. Xiu, W. Lyu, Z. Zhang, and C. Yuen, "Performance bounds for near-field localization with widely-spaced multi-subarray mmWave/THz MIMO," *IEEE Transactions on Wireless Communications*, vol. 23, no. 9, pp. 10 757–10 772, Mar. 2024.
- [13] S. Yang, C. Xie, W. Lyu, B. Ning, Z. Zhang, and C. Yuen, "Near-field channel estimation for extremely large-scale reconfigurable intelligent surface (XL-RIS)-aided wideband mmwave systems," *IEEE J. Sel. Areas Commun.*, vol. 42, no. 6, pp. 1567–1582, Apr. 2024.
- [14] S. K. Dehkordi, L. Pucci, P. Jung, A. Giorgetti, E. Paolini, and G. Caire, "Multistatic parameter estimation in the near/far field for integrated sensing and communication," *IEEE Trans. Wirel. Commun.*, vol. 23, no. 12, pp. 17 929–17 944, Sept. 2024.
- [15] A. Sakhnini, S. De Bast, M. Guenach, A. Bourdoux, H. Sahli, and S. Pollin, "Near-field coherent radar sensing using a massive MIMO communication testbed," *IEEE Trans. Wirel. Commun.*, vol. 21, no. 8, pp. 6256–6270, Feb. 2022.
- [16] C. Giovannetti, N. Decarli, and D. Dardari, "Performance bounds for velocity estimation with extremely large aperture arrays," *IEEE Wireless Commun. Lett.*, vol. 13, no. 12, pp. 3513–3517, Oct. 2024.
- [17] Z. Wang, X. Mu, and Y. Liu, "Near-field velocity sensing and predictive beamforming," *IEEE Trans. Veh. Technol.*, pp. 1–6, Sept. 2024.
- [18] H. Jiang, Z. Wang, and Y. Liu, "Near-field sensing enabled predictive beamforming: From estimation to tracking," *arXiv preprint arXiv:2408.02027*, 2024.
- [19] M. Rahal, B. Denis, M. F. Keskin, B. Uguen, and H. Wymeersch, "RIS-enabled NLoS near-field joint position and velocity estimation under user mobility," *IEEE J. Sel. Topics Signal Process.*, pp. 1–12, Jun. 2024.
- [20] J. Li and P. Stoica, *MIMO radar signal processing*. John Wiley & Sons, 2008.
- [21] M. A. Richards, J. Scheer, W. A. Holm, and W. L. Melvin, "Principles of modern radar," 2010.
- [22] M. I. Skolnik *et al.*, *Introduction to radar systems*. McGraw-hill New York, 1980, vol. 3.
- [23] M. Cui and L. Dai, "Near-field wideband beamforming for extremely large antenna arrays," *IEEE Trans. Wirel. Commun.*, vol. 23, no. 10, pp. 13 110–13 124, May 2024.
- [24] M. A. Richards *et al.*, *Fundamentals of radar signal processing*. McGraw-hill New York, 2005, vol. 1.
- [25] H.-A. Loeliger, "An introduction to factor graphs," *IEEE Signal Process. Mag.*, vol. 21, no. 1, pp. 28–41, Jan. 2004.
- [26] D. G. Tzikas, A. C. Likas, and N. P. Galatsanos, "The variational approximation for bayesian inference," *IEEE Signal Process. Mag.*, vol. 25, no. 6, pp. 131–146, Nov. 2008.
- [27] C. M. Bishop, "Pattern recognition and machine learning," *Springer google schola*, vol. 2, pp. 1122–1128, 2006.
- [28] M.-A. Badiu, T. L. Hansen, and B. H. Fleury, "Variational bayesian inference of line spectra," *IEEE Trans. Signal Process.*, vol. 65, no. 9, pp. 2247–2261, 2017.
- [29] Q. Zhang, J. Zhu, N. Zhang, and Z. Xu, "Multidimensional variational line spectra estimation," *IEEE Signal Process. Lett.*, vol. 27, pp. 945–949, May 2020.
- [30] K. V. Mardia and P. E. Jupp, *Directional statistics*. John Wiley & Sons, 2009.
- [31] F. Kschischang, B. Frey, and H.-A. Loeliger, "Factor graphs and the sum-product algorithm," *IEEE Trans. Inf. Theory*, vol. 47, no. 2, pp. 498–519, Aug. 2001.